[13] B.J. North, B.L. Marshall, M.T. Borra, et al., The human SIR2 ortholog, SIRT2, is an NAD+-dependent tubulin deacetylase, Mol. Cell. 11 (2003) 437–444.
[14] T. Nakagawa, D.J. Lomb, M. Haigis, et al., SIRT5 deacetylates carbamoyl phosphate synthetase 1 and regulates the urea cycle, Cell 137 (2009) 560–570.
[15] M.J. Jackson, A.L. Beaudet, W.E. O'Brien, Mammalian urea cycle enzymes, Annu. Rev. Genet. 20 (1986) 431–464.
[16] J.L. Deignan, S.D. Cederbaum, W.W. Grody, Contrasting features of urea cycle disorders in human patients and knockout mouse models, Mol. Genet. Metab. 93 (2008) 7–14.
[17] J. Miyazaki, K. Araki, E. Yamato, et al., Establishment of a pancreatic beta cell line that retains glucose-inducible insulin secretion: special reference to expression of glucose transporter isoforms, Endocrinology 127 (1990) 126–132.
[18] H. Niwa, K. Yamamua, J. Miyazaki, Efficient selection for high-expression transfectants with a novel eukaryotic vector, Gene 108 (1991) 193–200.
[19] S. Gupta, L.K. Rogers, S.K. Taylor, et al., Inhibition of carbamyl phosphate synthetase-I and glutamine synthetase by hepatotoxic doses of acetaminophen in mice, Toxicol. Appl. Pharmacol. 146 (1997) 317–327.
[20] L.A. Fahien, P.P. Cohen, A kinetic study of carbamyl phosphate synthetase, J. Biol. Chem. 239 (1964) 1925–1934.
[21] M. Hosokawa, B. Thorens, Glucose release from GLUT2-null hepatocytes: characterization of a major and a minor pathway, Am. J. Physiol. Endocrinol. Metab. 282 (2002) E794–801.
[22] D.M. Cyr, S.G. Egan, C.M. Brini, et al., On the mechanism of inhibition of gluconeogenesis and ureagenesis by sodium benzoate, Biochem. Pharmacol. 42 (1991) 645–654.
[23] D. Hunninghake, S. Grisolia, A sensitive and convenient micromethod for estimation of urea, citrulline, and carbamyl derivatives, Anal. Biochem. 16 (1966) 200–205.
[24] W.R. Fearon, The carbamido diacetyl reaction: a test for citrulline, Biochem. J. 33 (1939) 902–907.
[25] S. Nemoto, M.M. Fergusson, T. Finkel, Nutrient availability regulates SIRT1 through a forkhead-dependent pathway, Science 306 (2004) 2105–2108.
[26] S.C. Kim, R. Sprung, Y. Chen, et al., Substrate and functional diversity of lysine acetylation revealed by a proteomics survey, Mol. Cell. 23 (2006) 607–618.
[27] M. Gomez, A. Jorda, J. Cabo, et al., Effect of starvation on the N-acetylglutamate system of rat liver, FEBS. Lett. 156 (1983) 119–122.
[28] J.B. Tillman, J.M. Dhahbi, P.L. Mote, et al., Dietary calorie restriction in mice induces carbamyl phosphate synthetase I gene transcription tissue specifically, J. Biol. Chem. 271 (1996) 3500–3506.

Life Sciences 84 (2009) 876–881

Contents lists available at ScienceDirect

Life Sciences

journal homepage: www.elsevier.com/locate/lifescie

Effects of long-term dipeptidyl peptidase-IV inhibition on body composition and glucose tolerance in high fat diet-fed mice

Xibao Liu [a], Norio Harada [a], Shunsuke Yamane [a], Lisa Kitajima [b], Saeko Uchida [b], Akihiro Hamasaki [a], Eri Mukai [a,c], Kentaro Toyoda [a], Chizumi Yamada [a], Yuichiro Yamada [a,d], Yutaka Seino [a,e], Nobuya Inagaki [a,f,*]

[a] Department of Diabetes and Clinical Nutrition, Graduate School of Medicine, Kyoto University, Kyoto, Japan
[b] Molecular Function and Pharmacology Laboratories, Taisho Pharmaceutical Co., Ltd., Saitama, Japan
[c] Japan Association for the Advancement of Medical Equipment, Tokyo, Japan
[d] Department of Endocrinology and Diabetes and Geriatric Medicine, Akita University School of Medicine, Akita, Japan
[e] Kansai Electric Power Hospital, Osaka, Japan
[f] CREST of Japan Science and Technology Cooperation (JST), Kyoto, Japan

ARTICLE INFO

Article history:
Received 10 February 2009
Accepted 28 March 2009

Keywords:
Dipeptidyl peptidase-IV (DPP-IV)
DPP-IV inhibitor
Incretin
Glucagon-like peptide-1 (GLP-1)
Gastric inhibitory polypeptide (GIP)

ABSTRACT

Aim: Glucagon-like peptide-1 (GLP-1) and gastric inhibitory polypeptide (GIP) are major incretins associated with body weight regulation. Dipeptidyl peptidase-IV (DPP-IV) inhibitor increases plasma active GLP-1 and GIP. However, the magnitude of the effects of enhanced GLP-1 and GIP signaling by long-term DPP-IV inhibition on body weight and insulin secretion has not been determined. In this study, we compared the effects of long-term DPP-IV inhibition on body composition and insulin secretion of high fat diet (HFD)-fed wild-type (WT) and GLP-1R knockout (*GLP-1R*$^{-/-}$) mice.

Main methods: HFD-fed WT and *GLP-1R*$^{-/-}$ mice were treated with or without DPP-IV inhibitor by drinking water. Food and water intake and body weight were measured during 8 weeks of study. CT-based body composition analysis, Oral glucose tolerance test (OGTT), batch incubation study for insulin secretion and quantitative RT-PCR for expression of incretin receptors in isolated islets were performed at the end of study.

Key findings: DPP-IV inhibitor had no effect on food and water intake and body weight, but increased body fat mass in *GLP-1R*$^{-/-}$ mice. DPP-IV inhibitor-treated WT and *GLP-1R*$^{-/-}$ mice both showed increased insulin secretion in OGTT. In isolated islets of DPP-IV inhibitor-treated WT and *GLP-1R*$^{-/-}$ mice, glucose-induced insulin secretion was increased and insulin secretion in response to GLP-1 or GIP was preserved, without downregulation of incretin receptor expression.

Significance: Long-term DPP-IV inhibition may maintain body composition through counteracting effects of GLP-1 and GIP while improving glucose tolerance by increasing glucose-induced insulin secretion through the synergistic effects of GLP-1 and GIP.

Introduction

Oral glucose administration leads to much greater insulin release than the equivalent intravenous glucose challenge. Gut hormonal substances released in response to glucose include the incretins glucagon-like peptide-1 (GLP-1) and gastric inhibitory polypeptide /glucose-dependent insulinotropic peptide (GIP), which are responsible for ~50% of postprandial insulin release. GLP-1 and GIP potentiate glucose-induced insulin secretion from pancreatic β-cells by binding their respective receptors and subsequently increasing the intracellular cAMP concentration. In addition to their action on the enteroinsular axis, GLP-1 inhibits glucagon secretion (Komatsu et al. 1989), delays gastric emptying (Willms et al. 1996), decreases body weight through suppression of appetite (Turton et al. 1996), and suppresses β-cell apoptosis (Toyoda et al. 2008), while GIP enhances energy storage in adipocytes (Miyawaki et al. 2002) and calcium accumulation in bone (Tsukiyama et al. 2006). Thus, the incretins are associated with various systems of metabolic homeostasis, including that of both glucose and body weight.

However, the effects of GLP-1 and GIP are limited by their short half-life of a few minutes, which is primarily due to the action of dipeptidyl peptidase-IV (DPP-IV). DPP-IV is an enzyme distributed throughout the body including plasma and the endothelial lining of several organs, and cleaves two amino acids of biologically active peptides including GLP-1 and GIP by recognizing proline or alanine in the second N-terminal amino acid. The resulting N-terminal-truncated forms of GLP-1 and GIP are devoid of bioactivity. Since DPP-IV-deficient rodents show improved glucose tolerance and increased insulin secretion with elevated plasma active GLP-1 levels after oral glucose loading (Marguet et al. 2000; Nagakura et al. 2001), DPP-IV inhibitor and DPP-IV-resistant GLP-1

* Corresponding author. Department of Diabetes and Clinical Nutrition, Graduate School of Medicine, Kyoto University, 54 Shogoin Kawahara-cho, Sakyo-ku, Kyoto 606-8507, Japan. Tel.: +81 75 751 3560; fax: +81 75 751 4244.
E-mail address: inagki@metab.kuhp.kyoto-u.ac.jp (N. Inagaki).

0024-3205/$ – see front matter © 2009 Elsevier Inc. All rights reserved.
doi:10.1016/j.lfs.2009.03.022

receptor agonist are potential targets for the treatment of type 2 diabetes mellitus as a new class of antidiabetic agent. GLP-1 receptor agonist both increases insulin secretion and improves glucose tolerance and decreases body weight in rodents and humans (Szayna et al. 2000; Buse et al. 2004). DPP-IV inhibitor also increases insulin secretion and improves glucose tolerance, but its effect on body weight is controversial (Pospisilik et al. 2002; Lamont and Drucker 2008; Reimer et al. 2002; Ahrén et al. 2002). It is reported that DPP-IV inhibitor do not increase insulin secretion after glucose loading in GLP-1 receptor (GLP-1R)/GIP receptor (GIPR) double knockout (DIRKO) mice, indicating that both GLP-1 and GIP are critically involved in the insulinotropic action of long-term DPP-IV inhibition (Flock et al. 2007). However, the magnitude of the effects of enhanced GLP-1 and GIP signaling by long-term DPP-IV inhibition on body weight and insulin secretion has not been determined.

In the present study, we investigated the long-term effects of DPP-IV inhibition on body composition and insulin secretion using high fat diet (HFD)-fed wild-type (WT) and GLP-1R knockout (*GLP-1R*$^{-/-}$) mice.

Materials and methods

Animals

Mice (C57BL/6 background) were housed under a light/dark cycle of 12 h with free access to food and water. As ingestion of a meal rich in fat is a strong stimulus of incretin signaling (Harada et al. 2008), male WT and *GLP-1R*$^{-/-}$ mice were fed a high fat diet (45% fat, 20% protein and 35% carbohydrate by energy) from 7 weeks of age. Groups of treated HFD-fed WT and *GLP-1R*$^{-/-}$ mice received DPP-IV inhibitor in drinking water (0.5% W/V), while groups of untreated HFD-fed WT and *GLP-1R*$^{-/-}$ mice received drinking water without DPP-IV inhibitor. All the *GLP-1R*$^{-/-}$ mice were genotyped by Southern blot analysis. The DPP-IV inhibitor, provided by Taisho Pharmaceutical Co., Ltd., showed an inhibitory action on DPP-IV enzymatic activity against substrate H-Gly-Pro-7-amino-4-methyl coumarin (Gly-Pro-AMC) with IC_{50} (half maximal inhibitory concentration) of 0.0046 uM (Fukushima et al. 2008), while its IC_{50} on DPP-8 and DPP-9 were only 1.34 uM and 0.527 uM, respectively (unpublished data). Throughout the 8 weeks of study, water and food intake and body weight were measured once every 3 days. All mice care and procedures were approved by the Animal Care Committee of Kyoto University.

CT-based body composition analysis

The WT and *GLP-1R*$^{-/-}$ mice treated with or without DPP-IV inhibitor for 8 weeks were anesthetized and scanned along the body axis using LaTheta (LCT-100M) experimental animal CT system (Aloka, Tokyo, Japan). Contiguous 1-mm slice images of the whole abdominal cavity were used for quantitative assessment using LaTheta software (version 1.00). Weights of total fat mass, which comprises visceral fat mass and subcutaneous fat mass, and lean mass were quantitatively evaluated.

Oral glucose tolerance test (OGTT)

The WT and *GLP-1R*$^{-/-}$ mice treated with or without DPP-IV inhibitor for 8 weeks were fasted for 16 h and administered glucose (2 g/kg weight body) orally. Blood was collected from the orbital sinus of the mice at the indicated times (0, 15, 30, 60 and 120 min after glucose loading). Blood glucose levels were measured by the enzyme-electrode method. Plasma insulin levels were measured using an ELISA kit (Shibayagi, Gunma, Japan).

Measurement of plasma active GLP-1 levels and DPP-IV activity

For measurement of active GLP-1 levels, blood collected at 15 min after oral glucose loading was mixed with 2% EDTA· 4Na and 1% DPP-IV inhibitor (Linco Research, St Charles, MO). Active GLP-1 levels in plasma obtained by centrifugation (2000× g, 10 min, 4 °C) were measured using an active GLP-1 (7–36) ELISA kit (Linco Research).

Plasma DPP-IV activity was measured using a published method (Fukushima et al. 2008). In brief, 12.5 μl of plasma in duplicate was incubated with 37.5 μl of substrate cocktail (66.7 μM Gly-Pro-AMC, 25 mM HEPES, 140 mM NaCl, 26.6 mM $MgCl_2$, and 1% (w/v) BSA, pH 7.8) in the dark at room temperature for 5 min. The reaction was stopped by addition of 50 μl of 25% (v/v) acetic acid. Fluorescence was measured using a spectrofluorometer at excitation 360 nm/emission 465 nm. A standard curve was drawn using free AMC in standard buffer (25 mM HEPES, 140 mM NaCl, 20 mM $MgCl_2$, 1% (w/v) BSA, pH 7.8). DPP-IV activity (mU) is shown as the AMC (μM) generated in 1 ml plasma for 1 min of reaction time.

Measurement of insulin secretion in isolated islets

Islets were isolated from mice and preincubated at 37 °C for 30 min in 20 ml of Krebs-Ringer bicarbonate buffer (KRBB; 120 mM NaCl, 4.7 mM KCl, 1.2 mM $MgSO_4$, 1.2 mM KH_2PO_4, 2.4 mM $CaCl_2$, 20 mM $NaHCO_3$) supplemented with 10 mM HEPES and 0.2% (w/v) BSA and gassed with a mixture of 95% O_2 and 5% CO_2 (KRBB medium) containing 2.8 mM glucose. 10 size-matched islets collected in each tube were incubated at 37 °C for 30 min in 700 μl of KRBB medium containing 2.8 mM or 11.1 mM glucose with or without incretin peptides (100 nM human GLP-1 or 100 nM human GIP (Peptide Institute, Inc. Osaka, Japan)). Islets were then pelleted by centrifugation (9000× g, 2 min, 4 °C) and aliquots of the buffer were sampled. The amount of immunoreactive insulin was determined by radio-immunoassay (RIA). To determine insulin content, islets were homogenized in 400 μl acid-ethanol (37% HCl in 75% ethanol, 15:1000 (v/v)) and extracted at 4 °C overnight. The acidic extracts were dried by vacuum, reconstituted, and subjected to insulin measurement.

Measurement of mRNA expression of GLP-1R and GIPR in isolated islets

Measurement of mRNA expression of GLP-1R and GIPR was performed by quantitative RT-PCR as described previously (Harada et al. 2008). Briefly, total RNA was extracted from isolated islets with RNeasy mini kit (Qiagen, Valencia, CA) and treated with DNase (Qiagen). First strand cDNA was synthesized by SuperScript™ II Reverse Transcriptase system (Invitrogens, Grand Island, NY) according to manufacturer's instructions. SYBER Green PCR Master Mix (Applied Biosystems) was prepared for the PCR run. The PCR included 2 min at 50 °C and 10 min at 90 °C, followed by 50 cycles at 95 °C for 15 s and at 60 °C for 1 minute. The sequences of GLP-1R primers were 5′-CAACCGGACCTTTGATGACTA-3′ and 5′-GCTGTGCAGAACCGGTACAC-3′; the sequences of GIPR primers were 5′-CCTCCACTGGTCCCTACAC-3′ and 5′-GATAAACACCCTCCACCAGTAG-3′; the sequences of GAPDH primers were 5′-AAATGGTGAAGGTCGGTGTG-3′ and 5′-TCGTTGATGGCAACAATCTC-3′.

Statistical analyses

Data are expressed as means ± SE. Statistical analyses were performed by ANOVA and unpaired student's *t* test. *P* values < 0.05 were considered significant.

Results

Body weight and body composition of DPP-IV inhibitor-treated HFD-fed mice

Water intake, food intake, and body weight of HFD-fed WT and *GLP-1R*$^{-/-}$ mice with or without DPP-IV inhibitor administration were measured. In WT mice, water and food intake in DPP-IV

inhibitor-treated and untreated mice were similar during the 8 weeks of the study (Fig. 1A). In *GLP-1R*$^{-/-}$ mice, water and food intake in DPP-IV inhibitor-treated and untreated mice also were similar (Fig. 1A). A significant difference in body weight between DPP-IV inhibitor-untreated WT and *GLP-1R*$^{-/-}$ mice appeared from the 36th day (30.9 ± 1.3 g vs. 27.0 ± 0.6 g, $P<0.05$) (Fig. 1B). Body weight of WT mice and *GLP-1R*$^{-/-}$ mice was unaffected by DPP-IV inhibitor treatment during the 8 weeks of the study. To measure the effect of DPP-IV inhibitor on body composition, CT-based analysis was performed (Fig. 1C). In WT mice, there was no significant difference in body fat ratio between DPP-IV inhibitor-treated and untreated mice. However, the body fat ratio of DPP-IV inhibitor-treated *GLP-1R*$^{-/-}$ mice was significantly increased compared with that of untreated *GLP-1R*$^{-/-}$ mice (44.13 ± 1.55 vs. 32.60 ± 3.50, $P<0.05$).

OGTT of DPP-IV inhibitor-treated mice

In OGTT, blood glucose levels at 30 and 60 min were significantly lower in DPP-IV inhibitor-treated WT and *GLP-1R*$^{-/-}$ mice compared to those in untreated WT and *GLP-1R*$^{-/-}$ mice, respectively (Fig. 2A). In WT mice, the plasma insulin level of DPP-IV inhibitor-treated mice was 2.3 times higher at 15 min than that of untreated control mice ($P<0.05$), while in *GLP-1R*$^{-/-}$ mice, the plasma insulin levels of DPP-IV inhibitor-treated mice were 1.6 and 1.4 times higher at 15 and 30 min than those of untreated control mice, respectively ($P<0.05$) (Fig. 2B). In addition, the plasma insulin level of DPP-IV inhibitor-treated WT mice was 1.6 times higher at 15 min compared with that of DPP-IV inhibitor-treated *GLP-1R*$^{-/-}$ mice ($P<0.05$) (Fig. 2B).

We also measured plasma DPP-IV activity and active GLP-1 levels in WT and *GLP-1R*$^{-/-}$ mice at 15 min by OGTT. 75–80% of plasma DPP-IV activity in both untreated WT and *GLP-1R*$^{-/-}$ mice was inhibited by DPP-IV inhibitor treatment (Fig. 2C). Plasma levels of active GLP-1 were significantly elevated in DPP-IV inhibitor-treated WT and *GLP-1R*$^{-/-}$ mice compared to those in the respective untreated mice (Fig. 2D).

Insulin secretion and incretin receptor expression of islets isolated from DPP-IV inhibitor-treated mice

To determine insulin secretion in response to glucose and GLP-1 and GIP, batch incubation experiments were performed using islets isolated from WT and *GLP-1R*$^{-/-}$ mice after 8 weeks of treatment (Fig. 3A). In islets of WT mice, insulin secretion in response to 2.8 mM glucose was similar in DPP-IV inhibitor-treated and untreated mice. However, insulin secretion in response to 11.1 mM glucose, 11.1 mM glucose with GLP-1, and 11.1 mM glucose with GIP was significantly higher in DPP-IV inhibitor-treated mice than those in untreated mice. In addition, both GLP-1 and GIP augmented insulin secretion in the presence of 11.1 mM glucose in both DPP-IV inhibitor-treated and untreated mice. In islets of *GLP-1R*$^{-/-}$ mice, as in those of WT mice, insulin secretion in response to 2.8 mM glucose was similar in DPP-IV inhibitor-treated and untreated mice, and insulin secretion in response to 11.1 mM glucose, 11.1 mM glucose with GLP-1, and 11.1 mM glucose with GIP was significantly higher in DPP-IV inhibitor-treated mice than those in untreated mice. However, in *GLP-1R*$^{-/-}$ mice, potentiation of insulin secretion by incretin in the presence of 11.1 mM glucose was observed only by GIP and not by GLP-1 in both DPP-IV inhibitor-treated and untreated mice. Insulin content was similar among all groups of mice (data not shown).

To determine the effect of DPP-IV inhibitor treatment on the mRNA expression of GLP-1R and GIPR in islets, we performed quantitative RT-PCR after 8 weeks of study (Fig. 3B). The mRNA expression levels of GLP-1R and GIPR in DPP-IV inhibitor-treated and untreated WT mice were similar, as were total mRNA expression levels of GIPR in DPP-IV inhibitor-treated and untreated *GLP-1R*$^{-/-}$ mice.

Discussion

In the present study, we evaluated body composition and glucose control in the absence of the GLP-1 signaling using *GLP-1R*$^{-/-}$ mice treated with DPP-IV inhibitor for 8 weeks to clarify GLP-1 and GIP action under long-term DPP-IV inhibition.

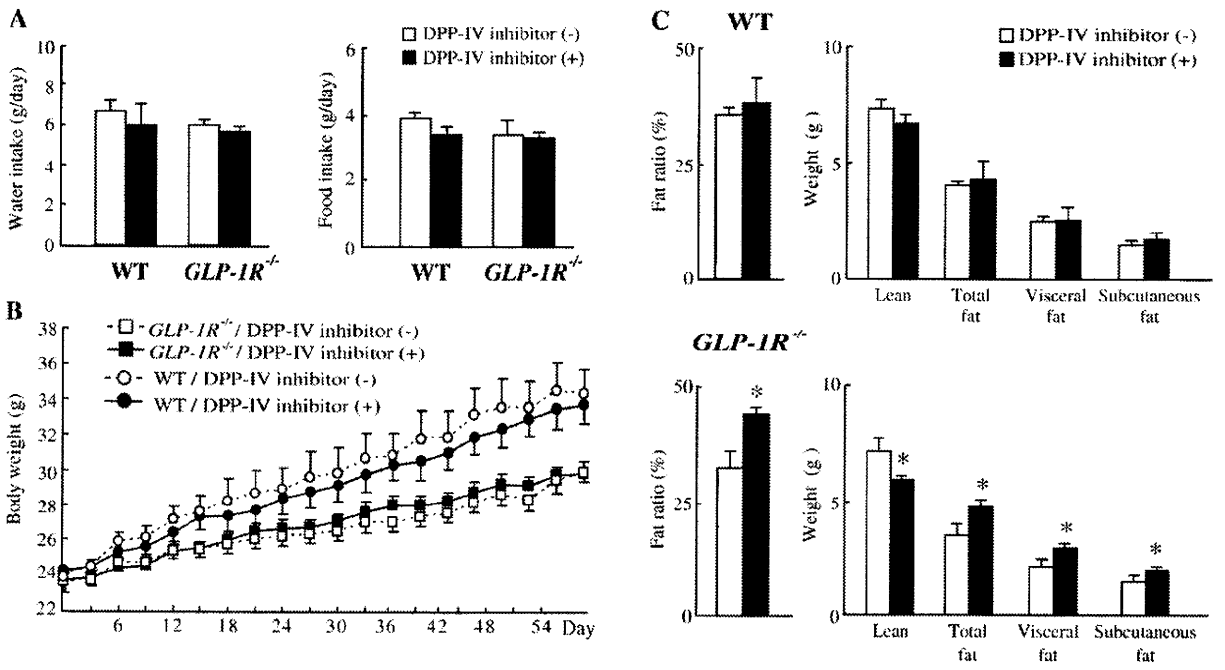

Fig. 1. Water and food intake, body weight and CT-based body composition analysis. (A) Water intake (left) and food intake (right) of WT and *GLP-1R*$^{-/-}$ mice treated with (filled) or without (open) DPP-IV inhibitor at the last week of study (average of 1 day). (B) Body weight change of WT (circle) and *GLP-1R*$^{-/-}$ (square) mice treated with (filled) or without (open) DPP-IV inhibitor. (C) CT-based body composition analysis of WT (upper) and *GLP-1R*$^{-/-}$ (lower) mice treated with (filled) or without (open) DPP-IV inhibitor. Fat ratio calculated as: total fat/(lean + total fat) × 100. Values are means ± SE. *$P<0.05$ vs. untreated mice ($n = 5$–6).

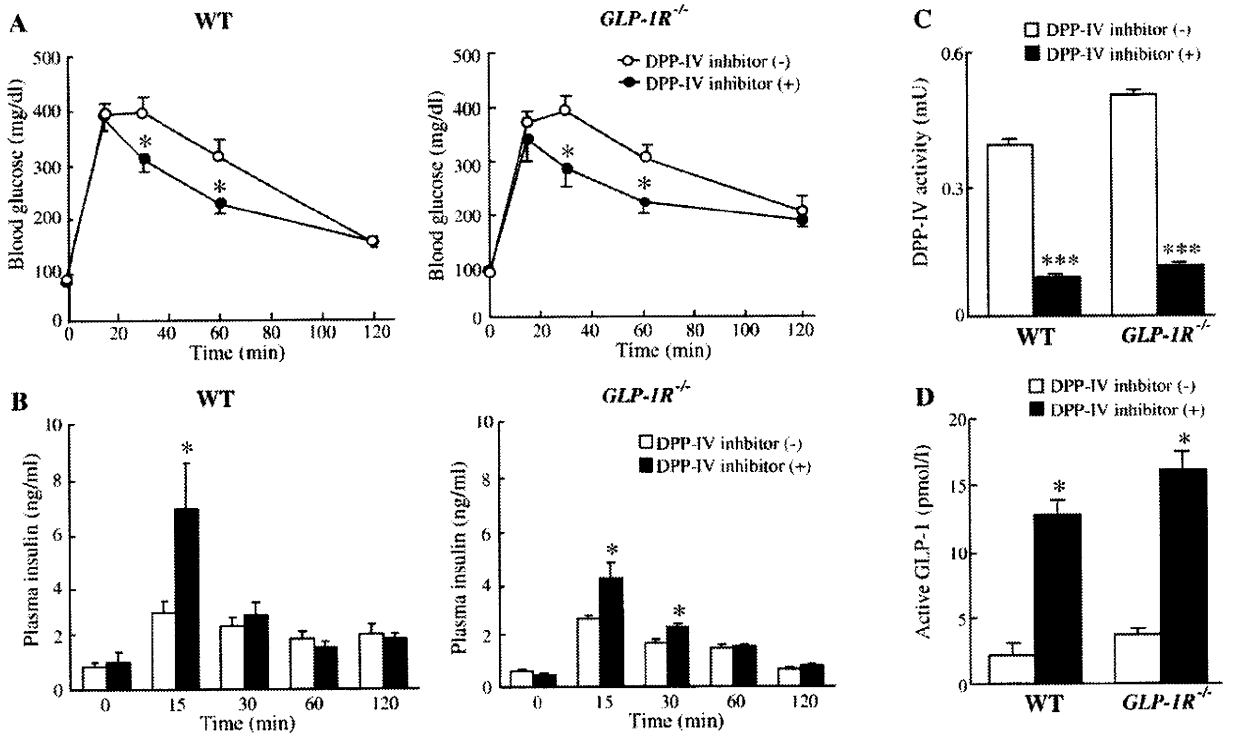

Fig. 2. OGTT. Blood glucose levels (A) and plasma insulin levels (B) of WT (left) and *GLP-1R*$^{-/-}$ (right) mice treated with (filled) or without (open) DPP-IV inhibitor after 8 weeks of study. Plasma DPP-IV activity (C) and plasma levels of active GLP-1 (D) at 15 min for WT and *GLP-1R*$^{-/-}$ mice treated with (filled) or without (open) DPP-IV inhibitor. Values are means ± SE. *$P<0.05$, ***$P<0.001$ vs. untreated mice ($n=5$–6).

HFD-fed DPP-IV-deficient rodents exhibit reduced food intake and resistance to development of obesity with elevated active GLP-1 levels (Yasuda et al. 2002; Conarello et al. 2003), and DPP-IV inhibitor has been shown to reduce body weight in some previous studies using rodent models (Pospisilik et al. 2002; Lamont and Drucker 2008). In the present study, no alteration in body weight was found after 8 weeks of DPP-IV inhibitor treatment either in HFD-fed WT or *GLP-1R*$^{-/-}$ mice, although 75–80% of plasma DPP-IV activity was inhibited and plasma active GLP-1 levels were significantly elevated after oral glucose loading. However, CT-based body composition analysis revealed that DPP-IV inhibitor treatment increased body fat mass in *GLP-1R*$^{-/-}$ mice but not in WT mice. DPP-IV is well known to be involved in inactivation of both GLP-1 and GIP, and plasma active GIP levels are elevated by treatment of DPP-IV inhibitor (Deacon et al. 2001). The receptor for GIP, differently from that for GLP-1, is expressed in adipocytes, and GIP directly facilitates energy accumulation in adipose tissue (Miyawaki et al. 2002; Naitoh et al. 2008). Our results suggest that fat accumulation is potentiated by fat-augmenting factors including GIP in the absence of the GLP-1 signaling under long-term DPP-IV inhibition. Thus, the lack of change in body weight and fat mass in DPP-IV inhibitor-treated WT mice may be due to the counteracting effects of enhanced GLP-1 and GIP signaling. In addition, *GLP-1R*$^{-/-}$ mice showed less body weight gain compared to that of WT mice, consistent with the previous report on *GLP-1R*$^{-/-}$

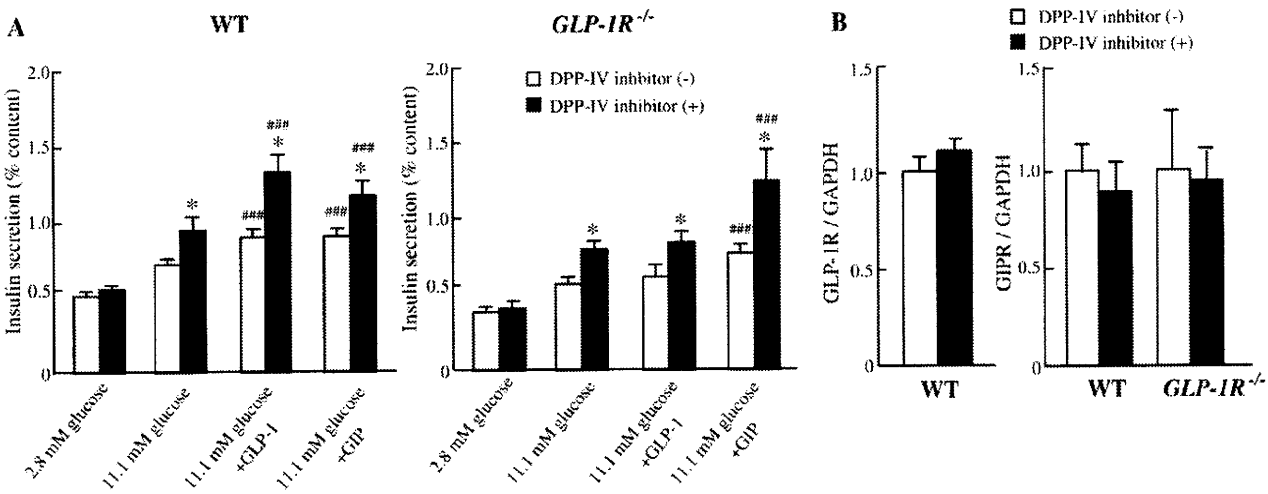

Fig. 3. Functional study of isolated islets. (A) Insulin secretion from islets isolated from WT (left) and *GLP-1R*$^{-/-}$ (right) mice treated with (filled) or without (open) DPP-IV inhibitor after 8 weeks of study. Values are means ± SE. *$P<0.05$ vs. untreated mice. ###$P<0.05$ vs. 11.1 mM glucose. (B) The mRNA expression of GLP-1R and GIPR in islets isolated from WT and *GLP-1R*$^{-/-}$ mice treated with (filled) or without (open) DPP-IV inhibitor. GLP-1R and GIPR mRNA levels were corrected for GAPDH mRNA levels, respectively. Data of DPP-IV inhibitor-treated mice is shown relative to untreated mice. Values are means ± SE. ($n=5$–8).

mice showing reduced body weight gain compared to that of WT mice, possibly due to enhanced locomotor activity and increased energy expenditure (Hansotia et al. 2007).

GLP-1 and GIP both are clearly involved in the effects of long-term DPP-IV inhibition on improved glucose tolerance, as DPP-IV inhibitor fails to increase insulin secretion and decrease plasma glucose after oral glucose loading in DIRKO mice (Flock et al. 2007). Our comparison in the present study of *GLP-1R*$^{-/-}$ mice and WT mice enables us to estimate the magnitude of the effects of enhanced GLP-1 and GIP by long-term DPP-IV inhibition on insulin secretion separately. Improved glucose tolerance and increased plasma insulin with elevated active GLP-1 levels were found in both DPP-IV inhibitor-treated WT and *GLP-1R*$^{-/-}$ mice by OGTT, indicating that GIP contributes to the insulinotropic effects of long-term DPP-IV inhibition in *GLP-1R*$^{-/-}$ mice. Moreover, blood insulin at 15 min in DPP-IV inhibitor-treated *GLP-1R*$^{-/-}$ mice was about half of that in DPP-IV inhibitor-treated WT mice. These results confirm that GLP-1 and GIP are important mediators of the insulinotropic effects of long-term DPP-IV inhibition. In addition, insulin secretion from islets in response to 11.1 mM glucose was increased in DPP-IV inhibitor-treated WT and *GLP-1R*$^{-/-}$ mice, indicating that glucose sensitivity of insulin secretion is augmented by long-term DPP-IV inhibitor administration unrelated to the GLP-1 signaling. However, the mechanism is not known. A recent report found that the glucose sensitivity of insulin secretion in isolated islets of mice improved after GLP-1 receptor agonist treatment due to augmented cAMP-induced activation of protein kinase A (PKA) through the GLP-1 receptor (Winzell and Ahrén 2008). It also was reported that activated PKA due to GLP-1 signaling increased expression of transcription factor pancreatic-duodenum homeobox-1 (PDX-1), translocation of PDX-1 from cytoplasm to nucleus, and phosphorylation of glucose transporter type 2 (GLUT2) in β-cells (Wang et al. 2001; Thorens et al. 1996). Thus, the increased glucose sensitivity of insulin secretion in islets unrelated to the GLP-1 signaling may be the result of augmented GIP signaling due long-term DPP-IV inhibition through similar mechanisms. Further study is required to clarify the augmentation of glucose sensitivity of islets after long-term DPP-IV inhibitor administration.

In addition to the plasma active incretin level, the expression of incretin receptors in islets also influences their insulinotropic effect (Lynn et al. 2001; Xu et al. 2007). Indeed, it has been reported that continuous GLP-1 stimulation results in desensitization of GLP-1R, which can subsequently reduce insulin secretion in response to GLP-1 in insulin-secreting cell lines (Widmann et al. 1996; Green et al. 2005). However, the expression of GLP-1R and GIPR in islets did not change in DPP-IV inhibitor-treated mice in the present study. Furthermore, insulin secretion in response to incretins was maintained in the islets of DPP-IV inhibitor-treated mice, demonstrating that sensitivity of the incretin receptors did not decrease even after 8 weeks of continuous incretin stimulation. These results suggest that the action of DPP-IV inhibitor in glucose control is preserved during long-term DPP-IV inhibitor administration.

Conclusion

Long-term DPP-IV inhibition does not alter body composition, possibly due to the counteracting effects of enhanced GLP-1 and GIP, but does improve glucose tolerance through the synergistic insulinotropic effects of enhanced GLP-1 and GIP, as well as by improved glucose responsiveness in pancreatic islets.

Acknowledgments

We thank Dr. Daniel. J. Drucker (Department of Medicine, The Banting and Best Diabetes Centre, Toronto General Hospital, University of Toronto, Toronto, Canada) for providing the *GLP-1R*$^{-/-}$ mice.

The funding of this study was supported by Scientific Research Grants from the Ministry of Education, Culture, Sports, Science, and Technology (Japan) and from the Ministry of Health, Labor, and Welfare (Japan).

References

Ahrén B, Simonsson E, Larsson H, Landin-Olsson M, Torgeirsson H, Jansson PA, Sandqvist M, Båvenholm P, Efendic S, Eriksson JW, Dickinson S, Holmes D. Inhibition of dipeptidyl peptidase IV improves metabolic control over a 4-week study period in type 2 diabetes. Diabetes Care 25 (5), 869–875, 2002.

Buse JB, Henry RR, Han J, Kim DD, Fineman MS, Baron AD. Exenatide-113 Clinical Study Group. Effects of Exenatide (Exendin-4) on glycemic control over 30 weeks in sulfonylurea-treated patients with type 2 diabetes. Diabetes Care 27 (11), 2628–2635, 2004.

Conarello SL, Li Z, Ronan J, Roy RS, Zhu L, Jiang G, Liu F, Woods J, Zycband E, Moller DE, Thornberry NA, Zhang BB. Mice lacking dipeptidyl peptidase IV are protected against obesity and insulin resistance. Proceedings of the National Academy of Sciences of the United States of America 100 (11), 6825–6830, 2003.

Deacon CF, Danielsen P, Klarskov L, Olesen M, Holst JJ. Dipeptidyl peptidase IV inhibition reduces the degradation and clearance of GIP and potentiates its insulinotropic and antihyperglycemic effects in anesthetized pigs. Diabetes 50 (7), 1588–1597, 2001.

Flock G, Baggio LL, Longuet C, Drucker DJ. Incretin receptors for glucagon-like peptide 1 and glucose-dependent insulinotropic polypeptide are essential for the sustained metabolic actions of Vildagliptin in mice. Diabetes 56 (12), 3006–3013, 2007.

Fukushima H, Hiratate A, Takahashi M, Mikami A, Saito-Hori M, Munetomo E, Kitano K, Chonan S, Saito H, Suzuki A, Takaoka Y, Yamamoto K. Synthesis and structure–activity relationships of potent 4-fluoro-2-cyanopyrrolidine dipeptidyl peptidase IV inhibitors. Bioorganic & Medicinal Chemistry 16 (7), 4093–4106, 2008.

Green BD, Liu HK, McCluskey JT, Duffy NA, O'Harte FP, McClenaghan NH, Flatt PR. Function of a long-term, GLP-1-treated, insulin-secreting cell line is improved by preventing DPP IV-mediated degradation of GLP-1. Diabetes, Obesity & Metabolism 7 (5), 563–569, 2005.

Hansotia T, Maida A, Flock G, Yamada Y, Tsukiyama K, Seino Y, Drucker DJ. Extrapancreatic incretin receptors modulate glucose homeostasis, body weight, and energy expenditure. The Journal of Clinical Investigation 117 (1), 143–152, 2007.

Harada N, Yamada Y, Tsukiyama K, Yamada C, Nakamura Y, Mukai E, Hamasaki A, Liu X, Toyoda K, Seino Y, Inagaki N. A novel gastric inhibitory polypeptide (GIP) receptor splice variant influences GIP sensitivity of pancreatic {beta}-cells in obese mice. American Journal of Physiology. Endocrinology and Metabolism 294 (1), E61–E68, 2008.

Komatsu R, Matsuyama T, Namba M, Watanabe N, Itoh H, Kono N, Tarui S. Glucagonostatic and insulinotropic action of glucagon-like peptide-1-(7-36) amide. Diabetes 38 (7), 902–905, 1989.

Lamont BJ, Drucker DJ. Differential antidiabetic efficacy of incretin agonists versus DPP-4 inhibition in high fat-fed mice. Diabetes 57 (1), 190–198, 2008.

Lynn FC, Pamir N, Ng EH, McIntosh CH, Kieffer TJ, Pederson RA. Defective glucose-dependent insulinotropic polypeptide receptor expression in diabetic fatty zucker rats. Diabetes 50 (5), 1004–1011, 2001.

Marguet D, Baggio L, Kobayashi T, Bernard AM, Pierres M, Nielsen PF, Ribel U, Watanabe T, Drucker DJ, Wagtmann N. Enhanced insulin secretion and improved glucose tolerance in mice lacking CD26. Proceedings of the National Academy of Sciences of the United States of America 97 (12), 6874–6879, 2000.

Miyawaki K, Yamada Y, Ban N, Ihara Y, Tsukiyama K, Zhou H, Fujimoto S, Oku A, Tsuda K, Toyokuni S, Hiai H, Mizunoya W, Fushiki T, Holst JJ, Makino M, Tashita A, Kobara Y, Tsubamoto Y, Jinnouchi T, Jomori T, Seino Y. Inhibition of gastric inhibitory polypeptide signaling prevents obesity. Nature Medicine 8 (7), 738–742, 2002.

Nagakura T, Yasuda N, Yamazaki K, Ikuta H, Yoshikawa S, Asano O, Tanaka I. Improved glucose tolerance via enhanced glucose-dependent insulin secretion in dipeptidyl peptidase IV-deficient Fischer rats. Biochemical and Biophysical Research Communications 284 (2), 501–506, 2001.

Naitoh R, Miyawaki K, Harada N, Mizunoya W, Toyoda K, Fushiki T, Yamada Y, Seino Y, Inagaki N. Inhibition of GIP signaling modulates adiponectin levels under high-fat diet in mice. Biochemical and Biophysical Research Communications 376 (1), 21–25, 2008.

Pospisilik JA, Stafford SG, Demuth HU, Brownsey R, Parkhouse W, Finegood DT, McIntosh CH, Pederson RA. Long-term treatment with the dipeptidyl peptidase IV inhibitor P32/98 causes sustained improvements in glucose tolerance, insulin sensitivity, hyperinsulinemia, and β-cell glucose responsiveness in VDF (fa/fa) zucker rats. Diabetes 51 (4), 943–950, 2002.

Reimer MK, Holst JJ, Ahrén B. Long-term inhibition of dipeptidyl peptidase IV improves glucose tolerance and preserves islet function in mice. European Journal of Endocrinology/European Federation of Endocrine Societies 146 (5), 717–727, 2002.

Szayna M, Doyle ME, Betkey JA, Holloway HW, Spencer RG, Greig NH, Egan JM. Exendin-4 decelerates food intake, weight gain, and fat deposition in Zucker rats. Endocrinology 141 (6), 1936–1941, 2000.

Thorens B, Dériaz N, Bosco D, DeVos A, Pipeleers D, Schuit F, Meda P, Porret A. Protein kinase A-dependent phosphorylation of GLUT2 in pancreatic beta cells. The Journal of Biological Chemistry 271 (14), 8075–8081, 1996.

Toyoda K, Okitsu T, Yamane S, Uonaga T, Liu X, Harada N, Uemoto S, Seino Y, Inagaki N. GLP-1 receptor signaling protects pancreatic beta cells in intraportal islet transplant by inhibiting apoptosis. Biochemical and Biophysical Research Communications 367 (4), 793–798, 2008.

Tsukiyama K, Yamada Y, Yamada C, Harada N, Kawasaki Y, Ogura M, Bessho K, Li M, Amizuka N, Sato M, Udagawa N, Takahashi N, Tanaka K, Oiso Y, Seino Y. Gastric

inhibitory polypeptide as an endogenous factor promoting new bone formation after food ingestion. Molecular Endocrinology 20 (7), 1644–1651, 2006.
Turton MD, O'Shea D, Gunn I, Beak SA, Edwards CM, Meeran K, Choi SJ, Taylor GM, Heath MM, Lambert PD, Wilding JP, Smith DM, Ghatei MA, Herbert J, Bloom SR. A role for glucagon-like peptide-1 in the central regulation of feeding. Nature 379 (6560), 69–72, 1996.
Wang X, Zhou J, Doyle ME, Egan JM. Glucagon-like peptide-1 causes pancreatic duodenal homeobox-1 protein translocation from the cytoplasm to the nucleus of pancreatic beta-cells by a cyclic adenosine monophosphate/protein kinase A-dependent mechanism. Endocrinology 142 (5), 1820–1827, 2001.
Widmann C, Dolci W, Thorens B. Desensitization and phosphorylation of the glucagon-like peptide-1 (GLP-1) receptor by GLP-1 and 4-Phorbol 12-Myristate 13-Acetate. Molecular Endocrinology 10 (1), 62–75, 1996.
Willms B, Werner J, Holst JJ, Orskov C, Creutzfeldt W, Nauck MA. Gastric emptying, glucose responses, and insulin secretion after a liquid test meal: Effects of exogenous glucagon-like peptide-1 (GLP-1)-(7–36) amide in type 2 (noninsulin-dependent) diabetic patients. The Journal of Clinical Endocrinology and Metabolism 81 (1), 327–332, 1996.
Winzell MS, Ahrén B. Durable islet effects on insulin secretion and protein kinase A expression following exendin-4 treatment of high-fat diet-fed mice. Journal of Molecular Endocrinology 40 (2), 93–100, 2008.
Xu G, Kaneto H, Laybutt DR, Duvivier-Kali VF, Trivedi N, Suzuma K, King GL, Weir GC, Bonner-Weir S. Downregulation of GLP-1 and GIP receptor expression by hyperglycemia: Possible contribution to impaired incretin effects in diabetes. Diabetes 56 (6), 1551–1558, 2007.
Yasuda N, Nagakura T, Yamazaki K, Inoue T, Tanaka I. Improvement of high fat-diet-induced insulin resistance in dipeptidyl peptidase IV-deficient Fischer rats. Life Sciences 71 (2), 227–238, 2002.

Physiol Genomics 40: 94–99, 2010.
First published October 27, 2009; doi:10.1152/physiolgenomics.00123.2009.

Identification and characterization of a novel *ABCA3* mutation

Sang-Kyu Park,[1,2,3]* Louella Amos,[1]* Aparna Rao,[1] Michael W. Quasney,[1,2,3] Yoshihiro Matsumura,[4] Nobuya Inagaki,[5] and Mary K. Dahmer[1,2,3]

[1]*Department of Pediatrics,* [2]*Children's Research Institute, and* [3]*Human and Molecular Genetics Center, Medical College of Wisconsin, Milwaukee, Wisconsin;* [4]*Department of Biochemistry and Molecular Biology, Oregon Health and Science University, Portland, Oregon; and* [5]*Department of Diabetes and Clinical Nutrition, Kyoto University, Kyoto, Japan*

Submitted 31 July 2009; accepted in final form 25 October 2009

Park SK, Amos L, Rao A, Quasney MW, Matsumura Y, Inagaki N, Dahmer MK. Identification and characterization of a novel *ABCA3* mutation. *Physiol Genomics* 40: 94–99, 2010. First published October 27, 2009; doi:10.1152/physiolgenomics.00123.2009.—Mutations in the gene coding for ATP-binding cassette protein A3 (ABCA3) are recognized as a genetic cause of lung disease of varying severity. Characterization of a number of mutant ABCA3 proteins has demonstrated that the mutations generally affect intracellular localization or the ability of the protein to hydrolyze ATP. A novel heterozygous mutation that results in the substitution of cysteine for arginine at amino acid 295 in ABCA3 was identified in a premature infant with chronic respiratory insufficiency and abnormal lamellar bodies. Sequencing of DNA performed in study participants demonstrated that this was a mutation and not a common variant. Plasmid vectors containing *ABCA3* with the identified novel mutation tagged with green fluorescent protein on the carboxy terminus were generated. The effect of the mutation on protein function was characterized by examining the glycosylation state of the mutant protein in transiently transfected HEK293 cells and by examining ATP hydrolysis activity of the mutant protein with a vanadate-induced nucleotide trapping assay in stably transfected HEK293 cells. The ABCA3 protein containing the R295C mutation undergoes normal glycosylation and intracellular localization but has dramatically reduced ATP hydrolysis activity (12% of wild type). The identification of one copy of this novel mutation in a premature infant with chronic respiratory insufficiency suggests that *ABCA3* haploinsufficiency together with lung prematurity may result in more severe, or more prolonged, respiratory failure.

chronic respiratory insufficiency; surfactant; pediatrics; lung disease

SURFACTANT IS ESSENTIAL for normal lung function partly by lowering alveolar surface tension and preventing end-expiratory atelectasis. Surfactant is found in lamellar bodies in type II pneumocytes and is composed of phospholipids and the surfactant-associated proteins SP-A, SP-B, SP-C, and SP-D. Inherited mutations in SP-B and SP-C are associated with respiratory failure (6, 10, 18). Loss-of-function mutations on both alleles of SP-B result in surfactant deficiency, severe neonatal lung disease, and in some instances death. SP-C deficiency is generally less severe, resulting in a spectrum of respiratory problems, ranging from neonatal disease to childhood interstitial lung disease.

Recently, mutations in the ATP-binding cassette protein A3 (ABCA3) gene have been recognized as another cause of surfactant deficiency and lung disease (1, 2, 10, 20). ABCA3 is a member of the ABC family of transmembrane proteins involved in the transport of a variety of substrates across membranes (11). ABC proteins bind and hydrolyze ATP, and hydrolysis of ATP is required for the protein to function as a transporter. ABCA3 is specifically found in the limiting membrane of surfactant-storing intracellular lamellar bodies in type II alveolar epithelial cells (16, 21). Recent evidence indicates that ABCA3 transports lipids essential for surfactant synthesis and function into lamellar bodies (5, 8, 15, 17).

Mutations in *ABCA3* have been found to cause lung disease of varying severity. Over 70 *ABCA3* mutations have been identified in full-term infants with respiratory failure and children with interstitial lung disease (10), although the functional impact of many of these mutants has not been explored. Little is known about the effect of *ABCA3* mutations on premature infants who are predisposed to chronic lung disease because of their prematurity, although there is one report suggesting that a single nucleotide polymorphism (SNP) in *ABCA3* may be associated with a prolonged course of respiratory distress syndrome (RDS) in very premature infants (12).

In the present study, we have identified a novel mutation in the gene coding for ABCA3 in a premature Hmong infant with chronic respiratory insufficiency. This mutation substitutes a cysteine for an arginine at amino acid position 295 in the first intracellular loop (ICL-1) of ABCA3. Functional analysis of this R295C mutation demonstrates that the mutation severely compromises the ability of the protein to hydrolyze ATP.

MATERIALS AND METHODS

Enrollment of subjects. Individuals of a Hmong community in Wisconsin eligible for enrollment included *1*) healthy unrelated adults ≥18 yr of age of Hmong descent on no medications or *2*) parents and relatives of the index case. Subjects were identified through community outreach and the parents of the index case. Subjects who could not speak English were excluded, as were individuals whose immediate family member or first-degree relative was already enrolled. Research personnel obtained written consent from eligible subjects, and a buccal swab was obtained. A unique code was applied to the swab, and no identifiers were obtained by the investigators, with the exception of the parents and relatives of the index case. This study was approved by the Institutional Review Board.

DNA analysis. Buccal swabs were stored at −20°C until extraction. DNA was extracted from buccal swabs with the Epicentre MasterAmp Buccal Swab DNA Extraction kit (MB79015) and stored at −80°C.

DNA samples were amplified in the region of the variant with AmpliTaq Gold polymerase (Applied Biosystems, Foster City, CA) and the primers 5′-TCACCTTGACACAGAAGAGCAG-3′ and 5′-AGTAAGACCCTGTCGAATGCAG-3′. The PCR reaction conditions were 96°C for 5 min followed by 40 cycles of 94°C for 30 s, 55°C for 30 s, 72°C for 45 s, followed by 72°C for 10 min. The PCR product (248 bp) was treated with ExoSAP-IT (USB, Cleveland, OH) and sequenced.

* S.-K. Park and L. Amos contributed equally to the project and authorship of the manuscript.

Address for reprint requests and other correspondence: M. K. Dahmer, Div. of Critical Care, Dept. of Pediatrics, Medical College of Wisconsin, 9000 West Wisconsin Ave., MS681, Milwaukee, WI 53201 (e-mail: mdahmer@mcw.edu).

Cell culture. HEK293 cells purchased from American Type Culture Collection (Manassas, VA) were maintained in Dulbecco's modified Eagle's medium (DMEM; Invitrogen, Carlsbad, CA) supplemented with penicillin (100 U/ml), streptomycin (100 μg/ml), 25 mM HEPES, and 10% fetal bovine serum (FBS) in a humidified atmosphere of 5% CO_2 at 37°C.

DNA construction. The R295C mutant was initially generated from the pEGFPN1-ABCA3-green fluorescent protein (GFP) construct (14) with the QuikChange II XL site-directed mutagenesis kit (Stratagene, La Jolla, CA) and the following primers: forward 5′-AGGCTGAAGGAGTACATGTGCATGATGGGGCTCAGCAG-3′ and reverse 5′-CTGCTGAGCCCCATCATGCACATGTACTCCTTCAGCCT-3′ (underlines indicate substituted nucleotides). A R295C-GFP construct in a pCAGIpuro vector was generated by inserting the coding region of ABCA3-R295C-GFP into the pCAGIpuro vector. Presence of the mutation in the pEGFN1-ABCA3-R295C-GFP and pCAGIpuro-ABCA3-R295C-GFP constructs was confirmed by sequencing.

Glycosylation of wild-type and mutant ABCA3-GFP proteins. Transient transfections of HEK293 cells with wild-type *ABCA3*-GFP and *ABCA3* mutants L101P-GFP, N568D-GFP, and L982P-GFP (14), as well as the new pEGFPN1 construct for R295C-GFP, were performed with FuGENE 6 transfection reagent (Roche Applied Science, Indianapolis, IN) as previously described (14). Briefly, for each experiment cells were seeded into 100-mm dishes at a density of 3×10^6/dish for the assay and cultured for 1 day, and each plate was then transfected with 6 μg of one of the plasmid vectors listed above. Cells were cultured for an additional 48 h and lysed, and membranes were prepared as described previously (14). Membrane protein (10 μg) was treated with 100 U of peptide N-glycosidase F (PNGase F) or 500 U of endoglycosidase H (Endo H) (New England Biolabs, Beverly, MA) for 30 min at 37°C in a total volume of 20 μl. The samples were then electrophoresed on 5% SDS-polyacrylamide gels, and immunoblot analysis was performed with anti-GFP monoclonal antibody (Santa Cruz Biotechnology, Santa Cruz, CA).

Stable transfection of wild-type and mutant ABCA3-GFP. Clonally selected HEK293 cell lines stably expressing wild-type or various mutant *ABCA3*-GFP genes were developed as previously described (14) and maintained in DMEM containing 2.5 μg/ml puromycin (Sigma, St. Louis, MO).

Vanadate-induced nucleotide trapping assay of wild-type and mutant ABCA3-GFP proteins. Vanadate-induced nucleotide trapping was performed with 8-azido-[α-^{32}P]ATP purchased from Affinity Labeling Technologies (ALT, Lexington, KY) as described previously (14). Samples were analyzed by SDS-PAGE on 5% polyacrylamide gel, electrotransferred onto nitrocellulose membranes (Bio-Rad, Hercules, CA), and quantified with a STORM 860 PhosphorImager system (Amersham Biosciences, Piscataway, NJ). Each experiment was performed on a different passage of stably transfected cell lines.

RESULTS

Identification of a novel R295C mutation. A Hmong male born at 25 wk of gestation (weighing 790 g) was intubated at birth and received surfactant therapy for RDS. He required high-frequency oscillatory ventilation for 2½ mo and conventional mechanical ventilation for 1 mo and was eventually transitioned to noninvasive ventilation. After a 4-mo hospitalization in the neonatal intensive care unit, he was discharged on oxygen therapy with a nasal cannula. Within 4 wk of discharge, he was hospitalized with worsening respiratory failure, increasing oxygen need, and poor weight gain. Chest computerized tomography demonstrated coarse interstitial opacities, cystic changes, and focal hyperinflation, while bronchoscopy revealed normal upper and lower airway anatomy. Despite appropriate medical therapies, the child was hospital-

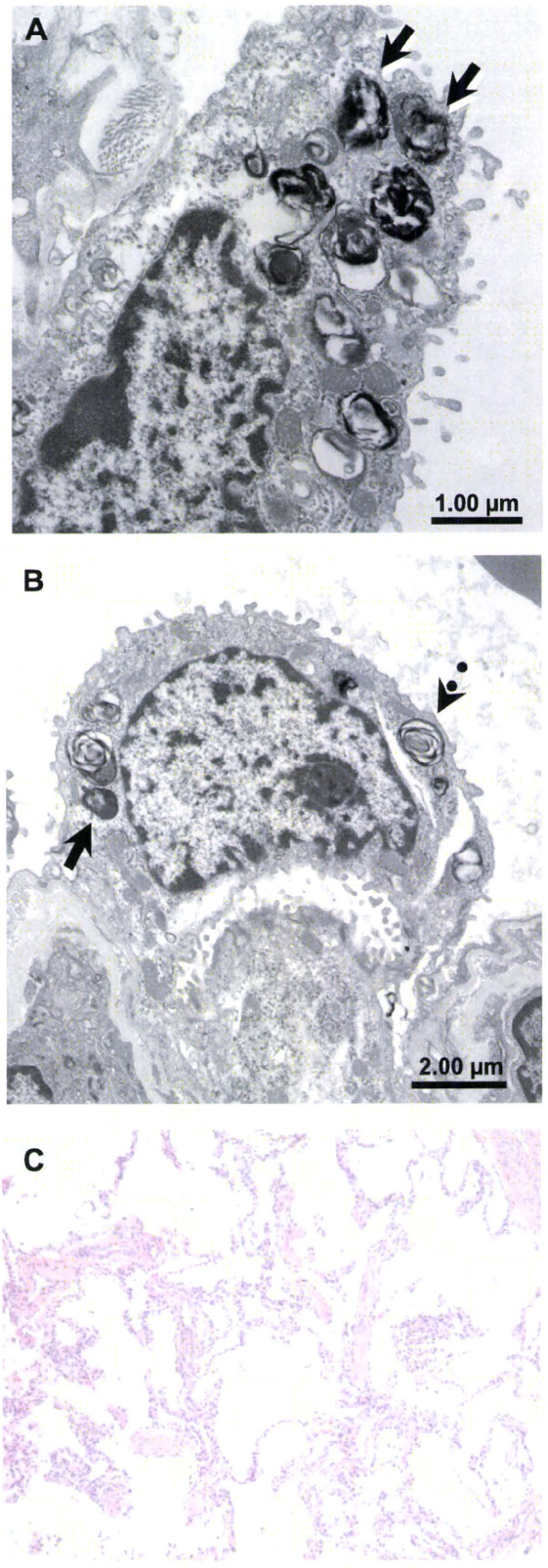

Fig. 1. Microscopy of the lung biopsy from a patient with chronic respiratory insufficiency. *A* and *B*: electron microscopy demonstrating abnormal lamellar bodies (solid arrows) and normal lamellar bodies (dashed arrows). Some cells have a combination of normal and abnormal lamellar bodies. *C*: hematoxylin and eosin staining (magnification ×20) demonstrating irregular dilatation and reduced number of peripheral alveoli with thickened smooth muscle in arterial walls.

ized during the majority of his first year of life for refractory respiratory insufficiency and eventually had a tracheostomy at age 1 yr. To determine whether the chronic respiratory insufficiency observed might be due to an inherited disorder resulting in surfactant deficiency, genetic testing (for mutations in the genes for SP-B, SP-C, and ABCA3 by sequencing of exons and splice sites) and a lung biopsy were performed. Lung biopsy demonstrated the presence of abnormal lamellar bodies (Fig. 1; some normal lamellar bodies were also observed) and chronic bronchopulmonary dysplasia (BPD) with persistent fetal pulmonary architecture. DNA sequencing revealed no mutations in the genes coding for SP-B and SP-C; however, the child was heterozygous for a novel variation in the *ABCA3* gene (replacement of a C with a T at nucleotide position 883). This change results in the replacement of arginine by cysteine at amino acid position 295. No other mutations in *ABCA3* were identified.

Although the R295C variant had not been observed in previously characterized populations, it was unclear whether the R295C variant was a common polymorphism in Hmong individuals or a clinically significant mutation. To determine whether the R295C variant was a polymorphism or a mutation, the frequency of this variant in the Hmong population was examined. DNA from individuals from the child's family, and from individuals in the Hmong community, was sequenced in the region of the variation. DNA samples from 90 of 91 individuals from the general Hmong population were sequenced successfully. None of these individuals had the R295C variant, indicating that this variation is indeed a mutation and not a polymorphism. Several members of the child's immediate family, including one of the parents, were heterozygous for the mutation.

Effects of ABCA3 R295C mutation on function. The R295C mutation is located in the first ICL (ICL-1) of the protein (Fig. 2*A*) and is adjacent to the previously reported mutant E292V (2). The R295C mutation resides in a region that is conserved in different members of the ABCA subfamily (Fig. 2*B*) and across ABCA3 homologs in vertebrates (Fig. 2*C*). Previous studies (4, 13, 14) have identified mutations that affect ABCA3 function by either altering intracellular localization (type I mutants) or impairing ATP hydrolysis activity (type II mutants).

To examine whether the intracellular localization of the R295C mutant was altered, the glycosylation state of the R295C mutant was characterized. Membranes from HEK293 cells expressing wild-type *ABCA3*-GFP, the R295C-GFP mutant, or several previously characterized mutants were examined for sensitivity to the glycosidases Endo H and PNGase F. In HEK293 cells, wild-type ABCA3-GFP is mainly localized in lysosomal organelles, mimicking the trafficking of ABCA3 to lamellar bodies in alveolar type II cells (14). Because Endo H only cleaves sugars from high-mannose oligosaccharides, and not from complex oligosaccharides, resistance to Endo H indicates that the protein is in post-Golgi membranes (presumably lamellar body-like organelles). After treatment

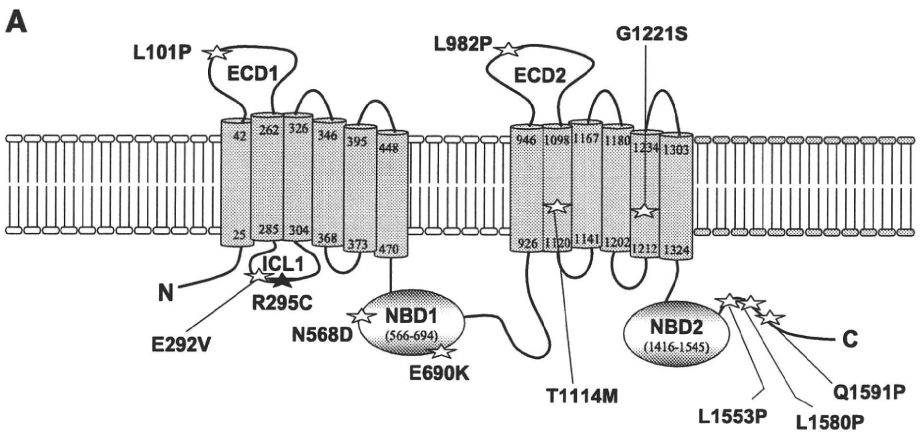

B

R295C

```
hABCA3    278 IARAVVQEKERRLKEYMRMMGLSSWLHWSAWFLL  311
hABCA1    655 IIKGIVYEKEARLKETMRIMGLDNSILWFSWFIS  688
hABCA2    723 TIQHIVAEKEHRLKEVMKTMGLNNAVHWVAWFIT  756
hABCA4    670 TVKSIVLEKELRLKETLKNQGVSNAVIWCTWFLD  703
hABCA7    565 TVKAVVREKETRLRDTMRAMGLSRAVLWLGWFLS  598
hABCA12  1084 FVKKLVYEKDLRLHEYMKMMGVNSCSHFFAWLIE 1117
```

C

R295C

```
Human        284  QEKERRLKEYMRMMGLSSWLHWSAW   308
Rat          284  QEKEKKLKEYMRMMGLSSWLHWSAW   308
Mouse        284  QEKEKKLKEYMRMMGLNSWLHWSAW   308
Chimpanzee   284  QEKERRLKEYMRMMGLSSWLHWSAW   308
```

Fig. 2. Schematic diagram of ATP-binding cassette protein A3 (ABCA3) and conservation of amino acids in the region of the R295C mutant. *A*: schematic diagram of the ABCA3 protein. ☆, Mutations reported previously; ★, novel mutant R295C. ECD1 and ECD2, extracellular domains; ICL-1, intracellular loop 1; NBD1 and NBD2, nucleotide binding domains. Type I mutations include L101P, L982P, L1553P, and Q1591P; type II mutations include E292V, N568D, E690K, T1114, G1221S, and L1580P (13, 14). *B*: alignment of sequences surrounding the R295C mutation in ICL-1 in various members of the ABCA subfamily. *C*: alignment of sequences surrounding the R295C mutation in human, rat, mouse, and chimpanzee.

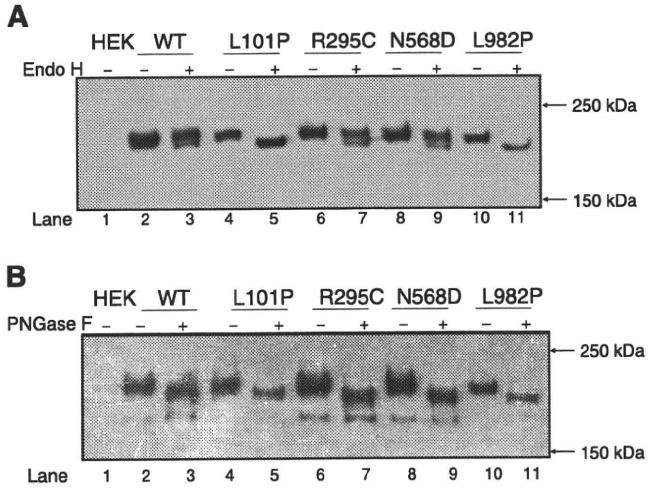

Fig. 3. Glycosylation of wild-type (WT) and mutant ABCA3-green fluorescent protein (GFP) proteins. *A*: 20 μg of membrane fraction from HEK293 cells transiently transfected with WT ABCA3-GFP (*lanes 2* and *3*) or with ABCA3-GFP mutants L101P (*lanes 4* and *5*), R295C (*lanes 6* and *7*), N568D (*lanes 8* and *9*), and L982P (*lanes 10* and *11*) were treated without (−) or with (+) endoglycosidase H (Endo H) and analyzed by 5% SDS-PAGE followed by immunoblotting with anti-GFP antibody. *Lane 1*, immunoblotting of untransfected HEK293 cells. *B*: WT ABCA3-GFP (*lanes 2* and *3*) or ABCA3-GFP mutants L101P (*lanes 4* and *5*), R295C (*lanes 6* and *7*), N568D (*lanes 8* and *9*), and L982P (*lanes 10* and *11*) were treated without (−) or with (+) peptide N-glycosidase F (PNGase F) and were then analyzed by 5% SDS-PAGE followed by immunoblotting with anti-GFP antibody. *Lane 1*, immunoblotting of untransfected HEK293 cells. Results from 1 representative experiment from a total of 3 separate experiments are shown.

with Endo H the wild-type ABCA3 protein is present as a doublet (Fig. 3*A*, *lane 3*), with much of the protein being resistant to Endo H, suggesting it is in post-Golgi membranes (Fig. 3*A*, compare *lanes 2* and *3*). This observation is consistent with previous reports. The R295C variant demonstrated a level of resistance to Endo H comparable to that of the wild-type protein (Fig. 3*A*, compare *lanes 6* and *7* to *lanes 2* and *3*), suggesting that the variant protein has undergone normal glycosylation and resides in post-Golgi membranes. As reported previously, the N568D variant shows resistance to Endo H (Fig. 3*A*, *lanes 8* and *9*) at a level similar to that of the wild-type protein; however, the L101P and L982P variants (Fig. 3*A*, *lanes 4* and *5* and *lanes 10* and *11*, respectively) show no Endo H resistance, indicating that these mutants have not left the endoplasmic reticulum (14). As expected, the wild-type and mutant ABCA3 proteins are all sensitive to PNGase F (Fig. 3*B*), which cleaves both high-mannose and complex oligosaccharide from N-linked glycoproteins.

To determine whether the R295C mutation affected the ATP hydrolysis activity of the R295C mutant, vanadate-induced nucleotide trapping with photoaffinity labeling of the trapped intermediate (3) was examined. In this assay, ATP hydrolysis with production of a stable intermediate can be assessed based on the intensity of photoaffinity labeling of the ABCA3 protein. As shown in Fig. 4*A*, the level of vanadate-induced nucleotide trapping in the R295C mutant was greatly reduced compared with that of the wild-type ABCA3 protein. The level of the ABCA3-R295C-GFP mutant protein was comparable to that of wild-type ABCA3-GFP as demonstrated in the anti-GFP immunoblot. Vanadate-induced nucleotide trapping was also decreased in the N568D mutant as reported previously (14). Quantitation of three independent experiments demonstrated that the degree of trapping in the R295C mutant was dramatically reduced to 12% of that of the wild type (Fig. 4*B*). These results indicate that the ability of the R295C mutant to hydrolyze ATP is severely impaired.

DISCUSSION

The results presented here demonstrate that R295C is a novel mutation that results in severely impaired ATP hydrolysis activity as indicated by the dramatic reduction in vanadate-induced nucleotide trapping. Other mutations in the ABCA3 protein also result in impaired ATP hydrolysis, including E292V, N568D, G1221S, L1580P, and T1114M (13, 14). The E292V mutation is in ICL-1 only three amino acids from the R295C mutation. Clearly, the presence of two mutations that affect ATP hydrolysis in this ICL suggests that the ICL is important for normal ATP hydrolysis activity and normal

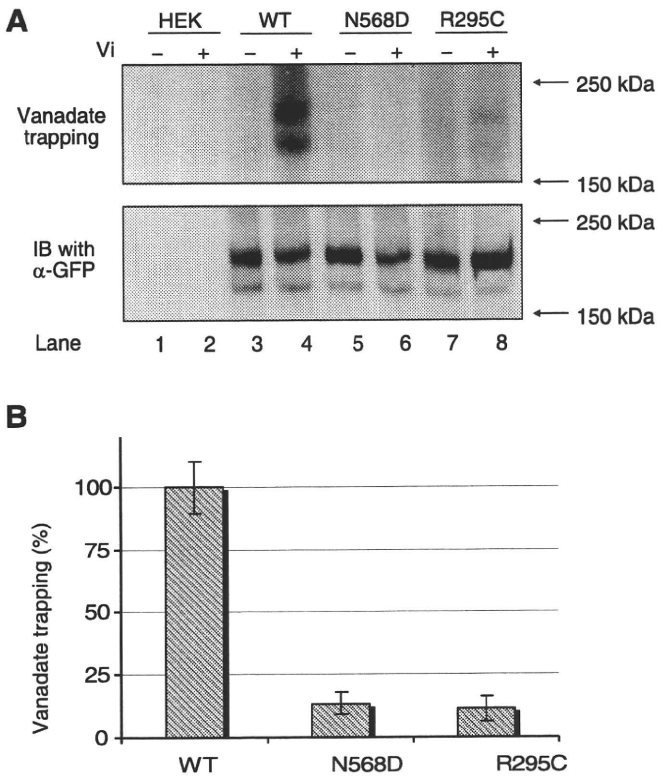

Fig. 4. Vanadate-induced nucleotide trapping in ABCA3-GFP and ABCA3-GFP mutants. *A*: 20 μg of membrane fraction from untransfected HEK293 cells (*lanes 1* and *2*), HEK293 cells stably expressing WT ABCA3-GFP (*lanes 3* and *4*), ABCA3-GFP mutants N568D (*lanes 5* and *6*), and R295C (*lanes 7* and *8*) were incubated with 20 μM 8-azido-[α-^{32}P]ATP in the absence (−) or presence (+) of 0.4 mM orthovanadate (Vi) and 3 mM $MgCl_2$ as described under MATERIALS AND METHODS. Photoaffinity-labeled ATP was detected by autoradiography (*top*) and immunoblotting (IB) using anti-GFP antibody (α-GFP) was used as a loading control (*bottom*). Results from 1 representative experiment from 3 separate experiments performed are shown. *B*: radioactivity of photoaffinity-labeled protein bands was measured and quantified (220 kDa of upper band intensities + 220 kDa of lower band intensities) with STORM 860 PhosphorImager. These were normalized to ABCA3-GFP protein from immunoblot (220 kDa of upper band intensities + 220 kDa of lower band intensities), and then radioactivity in the absence of orthovanadate was subtracted from that in the presence of orthovanadate. Data shown are means ± SD for 3 separate experiments (n = 3), 1 of which is shown in *A*.

functioning of the protein. This conclusion is also supported by the crystal structure of the bacterial ABC protein SAV1866, which suggests that ICLs transmit conformational changes important for function of the protein (7), and by the report of a mutation that reduces ATP hydrolysis activity in an ICL of multidrug resistance protein 1, another human ABC transporter protein (19).

The R295C mutation does not affect glycosylation and intracellular localization of the protein. The trafficking of proteins accompanies the processing of oligosaccharides from high-mannose to complex sugar types, with the presence of complex oligosaccharides indicating that the protein is in post-Golgi membranes. Resistance to Endo H has been demonstrated previously to be associated with localization of the ABCA3 protein to lamellar body-like organelles (14). Normal glycosylation and intracellular localization of the R295C mutant is indicated by the similar levels of sensitivity to Endo H and PNGase F observed for the wild-type ABCA3-GFP protein and the R295C mutant. The observation that a substantial portion of the R295C mutant protein is resistant to Endo H indicates that the mutation does not affect intracellular localization.

Although it is clear that the mutation impairs the function of the ABCA3 protein, the patient in whom this mutation was discovered is heterozygous for the mutation. While it is possible that either a mutation in a regulatory region of the noncoding sequence or an insertion or deletion of one or more exons might be present in the second copy of the *ABCA3* gene, it is more likely that the child has one normal copy of the *ABCA3* gene and consequently has normal as well as impaired ABCA3 protein. That the mutation has an effect on the cellular level of functional ABCA3 is indicated by the abnormal lamellar bodies observed in the patient's alveolar epithelial cells, although normal lamellar bodies are also present. Because one of the child's parents and two siblings also have the mutation and none has a history of severe lung disease, it is likely that there is sufficient functional ABCA3 present for normal lung function under normal conditions. However, the patient was born prematurely and was exposed to a number of stresses that are not seen in term infants, consequently haploinsufficiency (having just 1 functional copy of the gene) may explain the more severe injury and/or prolonged recovery period observed in this patient. Most premature infants require only supplemental oxygen on discharge from the neonatal intensive care unit; rarely do they need tracheostomy for long-term mechanical ventilation as was required for this patient. (By 2.5 yr old this patient had improved enough that a tracheostomy was no longer required.) This patient's haploinsufficiency may have caused surfactant dysfunction milder than would be expected in an individual homozygous for the mutation, but significant enough to cause chronic respiratory insufficiency in a premature infant. One possibility is that an interaction between the R295C mutation and the patient's prematurity resulted in the severe BPD observed. As has been suggested for individuals heterozygous for functional SP-B mutations (10), it is possible that for children heterozygous for a functional *ABCA3* mutation any environmental or developmental stress that alters *ABCA3* expression may result in more severe respiratory stress because of their already reduced level of functional ABCA3. Interestingly, the frequency of individuals heterozygous for the E292V mutation is elevated in a cohort of children with RDS, suggesting that a mutation in this region might impart increased genetic risk for respiratory insufficiency, even in heterozygotes (9).

In conclusion, clinical management of a premature infant with severe BPD and chronic respiratory failure led to the discovery of the novel *ABCA3* mutation R295C. This mutation, present in ICL-1, does not affect intracellular localization but severely impairs ATP hydrolysis activity of the ABCA3 mutant protein and is likely responsible for the aberrant lamellar bodies observed on lung biopsy. The identification of one copy of this novel mutation in a premature infant with chronic respiratory insufficiency suggests that *ABCA3* haploinsufficiency together with lung prematurity may result in more severe, or more prolonged, respiratory failure. Testing for *ABCA3* mutations in infants with refractory respiratory insufficiency or respiratory failure and a history of prematurity may help identify new mutations, clarify the function of ABCA3 and its various domains, and explain observed clinical deterioration despite appropriate medical management.

ACKNOWLEDGMENTS

We thank Daniel Merchant for excellent technical assistance and Dr. James F. Southern for providing histological analysis.

GRANTS

This work was supported, in part, by the Children's Research Institute at the Medical College of Wisconsin.

DISCLOSURES

No conflicts of interest are declared by the author(s).

REFERENCES

1. **Brasch F, Schimanski S, Muhlfeld C, Barlage S, Langmann T, Aslanidis C, Boettcher A, Dada A, Schroten H, Mildenberger E, Prueter E, Ballmann M, Ochs M, Johnen G, Griese M, Schmitz G.** Alteration of the pulmonary surfactant system in full-term infants with hereditary ABCA3 deficiency. *Am J Respir Crit Care Med* 174: 571–580, 2006.
2. **Bullard JE, Wert SE, Whitsett JA, Dean M, Nogee LM.** ABCA3 mutations associated with pediatric interstitial lung disease. *Am J Respir Crit Care Med* 172: 1026–1031, 2005.
3. **Carrier I, Julien M, Gros P.** Analysis of catalytic carboxylate mutants E552Q and E1197Q suggests asymmetric ATP hydrolysis by the two nucleotide-binding domains of P-glycoprotein. *Biochemistry* 42: 12875–12885, 2003.
4. **Cheong N, Madesh M, Gonzales LW, Zhao M, Yu K, Ballard PL, Shuman H.** Functional and trafficking defects in ATP binding cassette A3 mutants associated with respiratory distress syndrome. *J Biol Chem* 281: 9791–9800, 2006.
5. **Cheong N, Zhang H, Madesh M, Zhao M, Yu K, Dodia C, Fisher AB, Savani RC, Shuman H.** ABCA3 is critical for lamellar body biogenesis in vivo. *J Biol Chem* 282: 23811–23817, 2007.
6. **Cole FS, Nogee LM, Hamvas A.** Defects in surfactant synthesis: clinical implications. *Pediatr Clin North Am* 53: 911–917, 2006.
7. **Dawson RJ, Locher KP.** Structure of a bacterial multidrug ABC transporter. *Nature* 443: 180–185, 2006.
8. **Garmany TH, Moxley MA, White FV, Dean M, Hull WM, Whitsett JA, Nogee LM, Hamvas A.** Surfactant composition and function in patients with ABCA3 mutations. *Pediatr Res* 59: 801–805, 2006.
9. **Garmany TH, Wambach JA, Heins HB, Watkins-Torry JM, Wegner DJ, Bennet K, An P, Land G, Saugstad OD, Henderson H, Nogee LM, Cole FS, Hamvas A.** Population and disease-based prevalence of the common mutations associated with surfactant deficiency. *Pediatr Res* 63: 645–649, 2008.

10. **Hamvas A, Cole FS, Nogee LM.** Genetic disorders of surfactant proteins. *Neonatology* 91: 311–317, 2007.
11. **Kaminski WE, Piehler A, Wenzel JJ.** ABC A-subfamily transporters: structure, function and disease. *Biochim Biophys Acta* 1762: 510–524, 2006.
12. **Karjalainen MK, Haataja R, Hallman M.** Haplotype analysis of ABCA3: association with respiratory distress in very premature infants. *Ann Med* 40: 56–65, 2008.
13. **Matsumura Y, Ban N, Inagaki N.** Aberrant catalytic cycle and impaired lipid transport into intracellular vesicles in ABCA3 mutants associated with nonfatal pediatric interstitial lung disease. *Am J Physiol Lung Cell Mol Physiol* 295: L698–L707, 2008.
14. **Matsumura Y, Ban N, Ueda K, Inagaki N.** Characterization and classification of ATP-binding cassette transporter ABCA3 mutants in fatal surfactant deficiency. *J Biol Chem* 281: 34503–34514, 2006.
15. **Matsumura Y, Sakai H, Sasaki M, Ban N, Inagaki N.** ABCA3-mediated choline-phospholipids uptake into intracellular vesicles in A549 cells. *FEBS Lett* 581: 3139–3144, 2007.
16. **Mulugeta S, Gray JM, Notarfrancesco KL, Gonzales LW, Koval M, Feinstein SI, Ballard PL, Fisher AB, Shuman H.** Identification of LBM180, a lamellar body limiting membrane protein of alveolar type II cells, as the ABC transporter protein ABCA3. *J Biol Chem* 277: 22147–22155, 2002.
17. **Nagata K, Yamamoto A, Ban N, Tanaka AR, Matsuo M, Kioka N, Inagaki N, Ueda K.** Human ABCA3, a product of a responsible gene for ABCA3 for fatal surfactant deficiency in newborns, exhibits unique ATP hydrolysis activity and generates intracellular multilamellar vesicles. *Biochem Biophys Res Commun* 324: 262–268, 2004.
18. **Nogee LM.** Alterations in SP-B and SP-C expression in neonatal lung disease. *Annu Rev Physiol* 66: 601–623, 2004.
19. **Ren XQ, Furukawa T, Yamamoto M, Aoki S, Kobayashi M, Nakagawa M, Akiyama S.** A functional role of intracellular loops of human multidrug resistance protein 1. *J Biochem (Tokyo)* 140: 313–318, 2006.
20. **Shulenin S, Nogee LM, Annilo T, Wert SE, Whitsett JA, Dean M.** ABCA3 gene mutations in newborns with fatal surfactant deficiency. *N Engl J Med* 350: 1296–1303, 2004.
21. **Yamano G, Funahashi H, Kawanami O, Zhao LX, Ban N, Uchida Y, Morohoshi T, Ogawa J, Shioda S, Inagaki N.** ABCA3 is a lamellar body membrane protein in human lung alveolar type II cells. *FEBS Lett* 508: 221–225, 2001.

Rapamycin impairs metabolism-secretion coupling in rat pancreatic islets by suppressing carbohydrate metabolism

Makiko Shimodahira, Shimpei Fujimoto, Eri Mukai, Yasuhiko Nakamura, Yuichi Nishi, Mayumi Sasaki, Yuichi Sato, Hiroki Sato, Masaya Hosokawa, Kazuaki Nagashima, Yutaka Seino[1] and Nobuya Inagaki

Department of Diabetes and Clinical Nutrition, Graduate School of Medicine, Kyoto University, 54 Shogoin Kawahara-cho, Sakyo-ku, Kyoto 606-8507, Japan
[1]Kansai Electric Power Hospital, Osaka 553-0003, Japan
(Correspondence should be addressed to S Fujimoto; Email: fujimoto@metab.kuhp.kyoto-u.ac.jp)

Abstract

Rapamycin, an immunosuppressant used in human transplantation, impairs β-cell function, but the mechanism is unclear. Chronic (24 h) exposure to rapamycin concentration dependently suppressed 16·7 mM glucose-induced insulin release from islets (1·65±0·06, 30 nM rapamycin versus 2·35±0·11 ng/islet per 30 min, control, $n=30$, $P<0·01$) without affecting insulin and DNA contents. Rapamycin also decreased α-ketoisocaproate-induced insulin release, suggesting reduced mitochondrial carbohydrate metabolism. ATP content in the presence of 16·7 mM glucose was significantly reduced in rapamycin-treated islets (13·42 ±0·47, rapamycin versus 16·04±0·46 pmol/islet, control, $n=30$, $P<0·01$). Glucose oxidation, which indicates the velocity of metabolism in the Krebs cycle, was decreased by rapamycin in the presence of 16·7 mM glucose (30·1±2·7, rapamycin versus 42·2±3·3 pmol/islet per 90 min, control, $n=9$, $P<0·01$). Immunoblotting revealed that the expression of complex I, III, IV, and V was not affected by rapamycin. Mitochondrial ATP production indicated that the respiratory chain downstream of complex II was not affected, but that carbohydrate metabolism in the Krebs cycle was reduced by rapamycin. Analysis of enzymes in the Krebs cycle revealed that activity of α-ketoglutarate dehydrogenase (KGDH), which catalyzes one of the slowest reactions in the Krebs cycle, was reduced by rapamycin (10·08±0·82, rapamycin versus 13·82 ±0·84 nmol/mg mitochondrial protein per min, control, $n=5$, $P<0·01$). Considered together, these findings indicate that rapamycin suppresses high glucose-induced insulin secretion from pancreatic islets by reducing mitochondrial ATP production through suppression of carbohydrate metabolism in the Krebs cycle, together with reduced KGDH activity.
Journal of Endocrinology (2010) **204**, 37–46

Introduction

Rapamycin, an immunosuppressant used in human organ and tissue transplantation, exhibits a different mechanism of action from that of cyclosporine, tacrolimus, and corticosteroids. The agent is a macrolide that prevents T-cell activation through its inhibitory effect on serine/threonine kinase, the mechanistic target of rapamycin (MTOR). The insulin- and nutrient-signaling pathway through MTOR plays an important role in initiation of protein translation, a critical event in enhanced protein synthesis that leads to increased cell cycle progression and proliferation (McDaniel *et al.* 2002).

Brittle type 1 diabetes has been successfully treated by human islet transplantation using the Edmonton protocol, which includes use of rapamycin as an immunosuppressant (Shapiro *et al.* 2000). Some studies suggest rapamycin may be diabetogenic (Lu *et al.* 1994, Teutonico *et al.* 2005), and the effects of rapamycin on glucose homeostasis have been investigated. In skeletal muscle cells, long-term exposure to rapamycin decreases insulin-dependent uptake of glucose and glycogen synthesis and increases fatty acid oxidation (Sipula *et al.* 2006). Rapamycin also decreases insulin-mediated glucose uptake and insulin signaling in adipocytes (Taha *et al.* 1999, Cho *et al.* 2004). Interestingly, rapamycin both prevents β-cell mass expansion and impairs β-cell function (Bell *et al.* 2003, Zhang *et al.* 2006, Fraenkel *et al.* 2008).

In pancreatic β-cells, intracellular glucose metabolism regulates exocytosis of insulin granules according to metabolism-secretion coupling in which glucose-induced mitochondrial ATP production plays an essential role (Maechler & Wollheim 2001). Since depletion of mitochondrial DNA abolishes the glucose-induced ATP elevation, mitochondria clearly are a major source of ATP production in pancreatic β-cells (Kennedy *et al.* 1998, Tsuruzoe *et al.* 1998). Glucose-induced insulin secretion from β-cells is often impaired due to reduced glucose-induced ATP elevation by exposure to high concentrations of fuels including glucose, free fatty acids, and ketone body, and by administration of diabetogenic pharmacological agents (Fujimoto *et al.* 2007). Thus, reduced mitochondrial ATP production plays an important role in impaired glucose-induced insulin secretion.

Journal of Endocrinology (2010) **204**, 37–46
0022–0795/10/0204–037
DOI: 10.1677/JOE-09-0216
Online version via http://www.endocrinology-journals.org

Recently, several reports have shown that inhibition of MTOR by rapamycin decreases mitochondrial oxidative function using various materials including kidney mitochondria (Simon *et al.* 2003), Jurkat cells (Schieke *et al.* 2006), and skeletal tissue and cells (Cunningham *et al.* 2007). We investigated the effects of chronic exposure to rapamycin on metabolism-secretion coupling, especially on glucose metabolism in mitochondria, in pancreatic β-cells.

Materials and Methods

Materials

Rapamycin was purchased from Calbiochem (La Jolla, CA, USA). Disodium succinate, rotenone, pyruvate potassium, malate, and tetramethyl-*p*-phenyldiamine (TMPD) were purchased from Nacalai (Kyoto, Japan). Mouse monoclonal antibody to the subunits of the mitochondrial respiratory chain complex was obtained from Invitrogen. [5-^{3}H]-glucose, [U-^{14}C]-glucose, and anti-mouse IgG HRP-conjugated secondary antibody were obtained from GE Healthcare (Buckinghamshire, UK). Acetyl-CoA was obtained from Wako (Osaka, Japan). Luciferin–luciferase was obtained from Promega. All other reagents were obtained from Sigma Chemicals.

Animals

Male Wistar rats were obtained from Shimizu Co. (Kyoto, Japan). The animals were fed standard laboratory chow *ad libitum* and allowed free access to water in an air-conditioned room with a 12 h light:12 h darkness cycle until the experiments. All experiments were carried out with rats aged 8–11 weeks. The animals were maintained and used in accordance with the Guidelines for Animal Experiments of Kyoto University.

Islet isolation and culture

Islets of Langerhans were isolated from Wistar rats by collagenase digestion as previously described (Fujimoto *et al.* 1998). Isolated islets were cultured for 24 h in RPMI 1640 medium containing 10% FCS, 100 U/ml penicillin, 100 μg/ml streptomycin, and 5·5 mM glucose with or without rapamycin, at 37 °C in humidified air containing 5% CO_2.

Measurement of insulin release from isolated rat pancreatic islets, insulin content, and DNA content

Insulin release from intact islets was monitored using batch incubation as previously described (Fujimoto *et al.* 1998) using Krebs-Ringer bicarbonate buffer (KRBB) supplemented with 0·2% BSA (fraction V) and 10 mM HEPES adjusted to pH 7·4 (KRBB medium). After cultured islets were preincubated at 37 °C for 30 min in KRBB medium supplemented with 2·8 mM glucose, groups of five islets were batch incubated for 30 min in 0·7 ml KRBB medium containing 2·8 and 16·7 mM glucose with or without 100 μM α-tocopherol plus 200 μM ascorbate, or containing 2·8 and 16·7 mM α-ketoisocaproate (KIC). Before addition to KRBB medium, α-tocopherol was dissolved in ethanol at 1000-fold concentration. The same amount of ethanol was added to the control solution. At the end of the incubation period, the islets were pelleted by centrifugation, and aliquots of the buffer were sampled to determine the amount of immunoreactive insulin by RIA. After an aliquot of incubation medium for insulin release assay was taken, the islets remaining were lysed to determine insulin and DNA contents as previously described (Fujimoto *et al.* 2000).

Measurement of ATP content

ATP contents were determined as previously described (Kominato *et al.* 2008). Briefly, after groups of cultured islets were preincubated at 2·8 mM glucose for 30 min, groups of ten islets were incubated in tubes containing 0·5 ml KRBB medium supplemented with 2·8 or 16·7 mM glucose with or without 100 μM α-tocopherol plus 200 μM ascorbate at 37 °C for 30 min. Incubation was stopped by the addition of 0·1 ml of 2 M $HClO_4$. The contents of tubes were immediately mixed with vortex and sonicated in ice-cold water. The tubes were then centrifuged, and a fraction (0·4 ml) of the supernatant was mixed with 0·1 ml of 2 M HEPES and 0·1 ml of 1 M Na_2CO_3. The ATP concentration was measured by adding 0·2 ml luciferin–luciferase solution to a fraction sample (0·1 ml) in a bioluminometer (Luminometer Model 20e, Turner Designs, Sunnyvale, CA, USA). To draw a standard curve, blanks and ATP standards were run through the entire procedure including the extraction steps.

Measurement of glucose utilization and oxidation

Glucose utilization and oxidation were measured using the previously described method (Nabe *et al.* 2006). Briefly, cultured islets were preincubated in KRBB medium with 2·8 mM glucose at 37 °C for 30 min. For glucose utilization measurements, tubes containing 25 islets in 150 μl KRBB medium containing 2·8 or 16·7 mM glucose and 1·5 μCi [5-^{3}H] glucose were placed into glass vials containing 0·5 ml water. The capped vials were incubated at 37 °C for 90 min. After incubation was stopped by adding 50 μl of 1 M HCl into the incubation medium of the tubes without opening the caps, the capped vials were incubated overnight at 34 °C to allow $^{3}H_2O$ in the tubes to equilibrate with the water in the vial. Each tube was removed, and the disintegrations per minute of $^{3}H_2O$ in the water were counted. For oxidation measurements, procedures were the same as those for utilization measurements, except for the use of [U-^{14}C] glucose (0·5 μCi/tube) in place of [5-^{3}H] glucose and the use of 0·5 ml hydroxide of hyamine 10-X (Packard, Meriden, CT, USA) in place of 0·5 ml water.

Measurement of glucokinase activity

Glucokinase activity was measured by a fluorometric assay as previously described (Radu *et al.* 2005). Briefly, after cultured islets were preincubated with KRBB medium with 2·8 mM glucose, 100 islets were homogenized and the supernatants (islet extracts) were obtained from the homogenates by centrifugation. The glucose phosphorylation rate was estimated as the increase in NADH through the following reaction: glucose-6-phosphate + NAD^+ → 6-phosphoglucono-δ-lactone + NADH by NAD^+-dependent glucose-6-phosphate dehydrogenase (G6PDH). The enzyme reaction was performed using islet extracts in a solution containing NAD^+ and G6PDH supplemented with two concentrations (50 and 0·5 mM) of glucose at 37 °C for 1 h. NADH concentration was measured by fluorometry (Shimazu RF-5000, Kyoto, Japan).Glucokinase activity was determined by subtracting hexokinase activity measured at 0·5 mM glucose from the activity measured at 50 mM glucose.

Measurement of mitochondrial ATP production

Measurement of ATP production from mitochondrial fraction was performed as previously described (Takehiro *et al.* 2005). Briefly, to measure ATP production by oxidative phosphorylation, the reaction was started by adding mitochondrial suspension to prewarmed solution (37 °C) supplemented with the mitochondrial substrates, 50 μM ADP, and 1 μM diadenosine pentaphosphate (DAPP). DAPP is a specific inhibitor of adenylate kinase used to measure ATP production by oxidative phosphorylation exclusively. To normalize the mass of the intact mitochondria obtained, ATP production by adenylate kinase, one of the mitochondrial intermembrane kinases, was measured in the presence of ADP but without mitochondrial substrates or DAPP in parallel incubations. After reaction was stopped, the ATP concentration in the solutions was measured by adding luciferin–luciferase solution with a bioluminometer. ATP production was determined as the ratio of ATP production by oxidative phosphorylation to that by adenylate kinase.

Western blotting of mitochondrial respiratory chain complexes

After washing with ice-cold PBS, the cultured islets were solubilized in ice-cold lysis buffer (10 mM Tris (pH 7·2), 100 mM NaCl, 1 mM EDTA, 1% Nonidet P-40, and 0·5% sodium deoxycholate) containing protease inhibitor cocktail (Complete; Roche) with sonication (5 s pulse, five times). Protein content of the supernatant was measured and adjusted by Bradford method. The supernatant was dissolved in the same amount of SDS-PAGE sample buffer containing 100 mM Tris–HCl (pH 6·80), 4% SDS, 12% 2-mercaptoethanol, 20% glycerol, and 1% bromophenol blue and boiled for 5 min at 95 °C. The samples were subjected to electrophoresis on 12% SDS–polyacrylamide gels and transferred onto nitrocellulose membrane (Schleicher & Schuell, Keene, NH, USA). After blocking with TBS containing 0·1% Tween 20 and 5% skimmed milk (blocking buffer) for 1 h at 4 °C, blotted membranes were incubated overnight at 4 °C with mouse monoclonal anti-complex I (39 kDa subunit), anti-complex III (core II), anti-complex IV (subunit I), or anti-complex V (subunit α) of mitochondrial respiratory chain antibody at 1:1000 dilution in blocking buffer, and subsequently with anti-mouse IgG HRP-conjugated secondary antibody diluted 1:5000 at room temperature for 1 h prior to detection using ECL (GE Healthcare). In the same membrane, the process was repeated for β-actin at 1:5000 dilution of the antibody. Band intensities were quantified with Multi Gauge software (Fujifilm, Tokyo, Japan).

Measurement of activities of enzymes in Krebs cycle

Mitochondrial fraction obtained as described above was sonicated in ice-cold solution containing (mM) 180 KCl, 5 morpholinepropanesulfonic acid, and 2 EDTA adjusted to pH 7·40 and then diluted to each reaction mixture. Enzyme activities including NAD^+-linked isocitrate dehydrogenase (NAD-ICDH), aconitase, α-ketoglutarate dehydrogenase (KGDH), and malate dehydrogenase (MDH) were measured as previously described (Nulton-Persson & Szweda 2001). NAD-ICDH activities were measured as the rate of NAD^+ reduction in solution A containing (mM) 25 KH_2PO_4, 0·5 EDTA, and 0·01% Triton X-100 adjusted to pH 7·25 supplemented with 2·5 mM isocitrate, 40 μM rotenone, 5 mM $MgCl_2$, and 1 mM NAD^+. Aconitase activities were measured as the rate of $NADP^+$ reduction in solution A with 5 mM citrate, 0·6 mM $MgCl_2$, 1·0 U/ml NADP-ICDH, and 0·2 mM $NADP^+$. KGDH activities were measured as the rate of NAD^+ reduction in solution A with 2·5 mM α-ketoglutarate, 40 μM rotenone, 5·0 mM $MgCl_2$, 1 mM NAD^+, 0·1 mM CoA, and 0·2 mM thymine pyrophosphate (TPP). MDH activities were measured as the rate of NAD^+ reduction in solution A with 2·5 mM malate, 40 μM rotenone, 5 mM $MgCl_2$, 10 mM NAD^+, 0·3 mM acetyl-CoA, and 1 U/ml citrate synthase. Enzyme activities of pyruvate dehydrogenase (PDH) were measured as total PDH complex activity (Schwab *et al.* 2005) as the rate of *p*-iodonitrotetrazolium violet (INT) reduction in a reaction mixture containing 5 mM L-carnitine, 1·0 mM $MgCl_2$, 2·5 mM NAD^+, 0·1 mM CoA, 5 mM pyruvate, 0·2 mM TPP, 0·1% Triton X-100, 1 g/l BSA, 0·6 mM INT, and 6·5 mM phenazine methosulfate. All enzyme assays were performed at 25 °C.

Statistical analysis

The data are expressed as the mean ± S.E.M. Statistical significance was calculated by unpaired Student's *t*-test. $P<0·05$ was considered significant.

Results

Effect of chronic exposure to rapamycin on glucose-induced insulin release, insulin content, and DNA content in islets

Chronic (24 h) exposure to rapamycin (10, 30, and 100 nM) concentration dependently suppressed 16·7 mM glucose-induced insulin release (1·94±0·09, 10 nM; 1·65±0·06, 30 nM; 1·50±0·06, 100 nM rapamycin versus 2·35 ±0·11 ng/islet per 30 min, control, $n=30$, $P<0·01$ respectively) but did not affect basal insulin release in the presence of 2·8 mM glucose (Fig. 1A). Insulin secretion divided by insulin content also demonstrates that rapamycin suppresses glucose-induced insulin secretion (Fig. 1A). Insulin and DNA contents were not affected by 24-h exposure to 10, 30, and 100 nM rapamycin (Table 1), indicating that these concentrations of rapamycin do not reduce islet β-cell mass. Reactive oxygen species (ROS) scavengers did not affect suppressed glucose-induced insulin secretion by rapamycin (1·60±0·10, 30 nM rapamycin versus 1·69±0·10 ng/islet per 30 min, 30 nM rapamycin with α-tocopherol plus ascorbate, $n=10$, not significant).

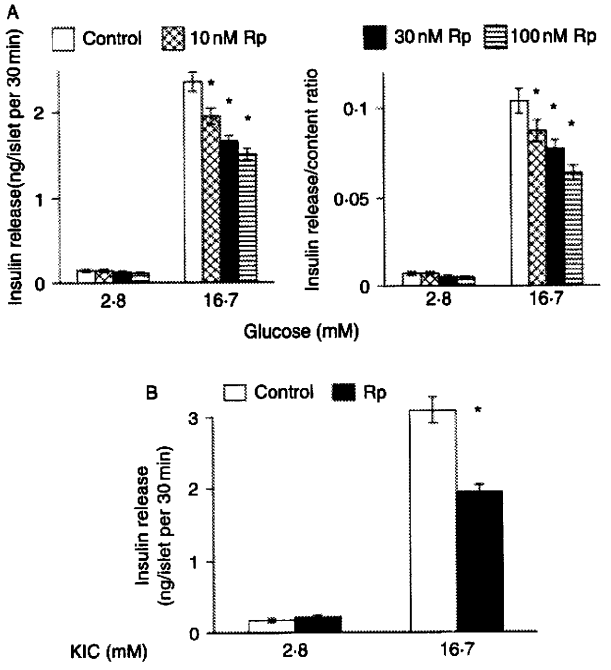

Figure 1 Effects of chronic exposure to rapamycin (Rp) on fuel secretagogue-induced insulin release from islets. (A) High (16·7 mM) glucose-induced and basal insulin release in control and Rp-treated islets. Islets were cultured with 10, 30, and 100 nM Rp or without Rp for 24 h. After cultured islets were preincubated with 2·8 mM glucose for 30 min, they were incubated with 2·8 and 16·7 mM glucose. Insulin secretions are presented as insulin secretion for 30 min/islet (right) and as the ratio of insulin secretion for 30 min to insulin content (left). Values represent mean±S.E.M. of 30 determinations. *$P<0·01$ versus corresponding control. (B) High KIC (16·7 mM)-induced and basal insulin release in control and Rp-treated islets. Islets were cultured with or without 30 nM Rp for 24 h. After cultured islets were preincubated with 2·8 mM glucose for 30 min, they were incubated with 2·8 and 16·7 mM KIC. Values represent mean±S.E.M. of 18 determinations. *$P<0·01$ versus corresponding control.

Table 1 Effect of chronic exposure to rapamycin on insulin content and DNA content. At the end of experiments indicated in Fig. 1A, insulin content and DNA content in islets were determined. Values represent mean±S.E.M. of 60 determinations

	Insulin content (ng/islet)	**DNA content** (ng/islet)
Experimental condition during culture		
Control	24·7±1·0	14·6±0·4
10 nM rapamycin	24·1±1·0	14·5±0·4
30 nM rapamycin	24·5±1·1	15·0±0·5
100 nM rapamycin	23·7±0·8	14·1±0·3

Effect of chronic exposure to rapamycin on KIC-induced insulin release

To characterize metabolic fuel-induced insulin release independent of glycolysis, KIC-induced insulin release from rapamycin-treated islets was examined. Chronic exposure to 30 nM rapamycin decreased high KIC-induced insulin release (1·93±0·10, rapamycin versus 3·09±0·18 ng/islet per 30 min, control, $n=18$, $P<0·01$; Fig. 1B).

Effect of rapamycin on ATP content

ATP content was greater in control islets incubated with 16·7 mM glucose than in control islets incubated with 2·8 mM glucose (11·97±0·35, 2·8 mM glucose versus 16·04±0·46 pmol/islet, 16·7 mM glucose, $n=30$, $P<0·01$; Fig. 2). ATP content in the presence of 16·7 mM glucose

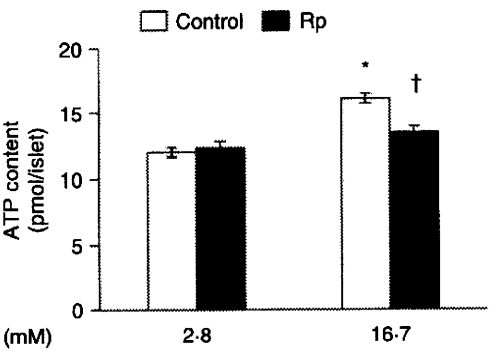

Figure 2 Effects of chronic exposure to rapamycin (Rp) on ATP contents in islets. Islets were cultured with or without 30 nM Rp for 24 h. After cultured islets were preincubated with 2·8 mM glucose for 30 min, and then incubated with 2·8 and 16·7 mM glucose for 30 min, ATP contents were determined. Values represent mean ±S.E.M. of 30 determinations. *$P<0·01$ versus control with 2·8 mM glucose. †$P<0·01$ versus control with 16·7 mM glucose.

was significantly reduced in rapamycin-treated islets (13·42 ±0·47 pmol/islet, 16·7 mM glucose, rapamycin versus 16·7 mM glucose, control, $n=30$, $P<0·01$), but that in the presence of 2·8 mM glucose was not affected by rapamycin (Fig. 2). ROS scavengers did not affect the suppressed ATP content in the presence of high glucose by rapamycin (13·27 ±0·92, 30 nM rapamycin versus 14·58±0·82 pmol/islet, 30 nM rapamycin with α-tocopherol plus ascorbate, $n=10$, not significant).

Effects of rapamycin on glucose utilization and glucose oxidation

Glucose utilization was greater in islets incubated with 16·7 mM glucose than that in islets incubated with 2·8 mM glucose in both control (33·0±1·8, 2·8 mM glucose versus 98·4±5·0 pmol/islet per 90 min, 16·7 mM glucose, $n=15$, $P<0·01$) and rapamycin-treated islets (28·1±1·7, 2·8 mM glucose versus 75·1±2·6 pmol/islet per 90 min, 16·7 mM glucose, $n=15$, $P<0·01$). Glucose utilization in the presence of 16·7 mM glucose was significantly reduced in rapamycin-treated islets ($P<0·01$), but that in the presence of 2·8 mM glucose was not affected by rapamycin (Fig. 3A).

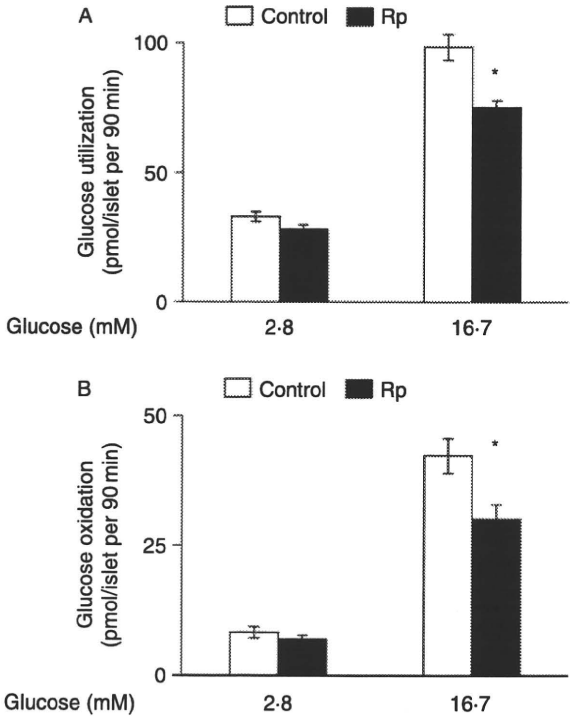

Figure 3 Effects of chronic exposure to rapamycin (Rp) on glucose utilization and oxidation in islets. Islets were cultured with or without 30 nM Rp for 24 h. After cultured islets were preincubated with 2·8 mM glucose for 30 min, they were incubated with 2·8 and 16·7 mM glucose for 90 min. (A) Glucose utilization. Values represent mean±S.E.M. of 15 determinations. *$P<0·01$ versus corresponding control. (B) Glucose oxidation. Values represent mean±S.E.M. of nine determinations. *$P<0·01$ versus corresponding control.

Glucose oxidation was greater in islets incubated with 16·7 mM glucose than that in islets incubated with 2·8 mM glucose in both control (8·1±1·1, 2·8 mM glucose versus 42·2±3·3 pmol/islet per 90 min, 16·7 mM glucose, $n=9$, $P<0·01$) and rapamycin-treated islets (6·8±0·7, 2·8 mM glucose versus 30·1±2·7 pmol/islet per 90 min, 16·7 mM glucose, $n=9$, $P<0·01$). Glucose oxidation in the presence of 16·7 mM glucose was significantly reduced in rapamycin-treated islets ($P<0·01$), but that in the presence of 2·8 mM glucose was not affected by rapamycin (Fig. 3B). Glucose oxidation in the presence of 16·7 mM glucose declined 77% by 100 nM antimycin A, which is comparable with the reduction by rapamycin treatment. In the same condition, glucose utilization with high glucose also declined 78% by antimycin A (Table 2).

Effect of rapamycin on glucokinase activity

Glucokinase activity was not affected by rapamycin treatment (87·4±10·4, rapamycin versus 75·4±14·8 pmol/islet per 60 min, control, $n=3$, not significant).

Effect of rapamycin on expression of mitochondrial respiratory chain complexes

Immunoblotting using lysates of whole islets revealed that rapamycin did not affect expression of complex I, III, IV, and V of the mitochondrial respiratory chain proteins (Fig. 4).

Effect of rapamycin on ATP production by mitochondria from islets

ATP production by mitochondria from control and rapamycin-cultured islets in the presence of various substrates and inhibitors is shown in Table 3. Antimycin A, a complex III inhibitor in the respiratory chain, inhibited ATP production dramatically in the presence of succinate in mitochondria from both control and rapamycin-cultured islets. Mitochondrial ATP production of rapamycin-cultured islets was similar to that of control islets in the presence of

Table 2 Effect of antimycin A on glucose oxidation and glucose utilization. Islets were cultured without rapamycin for 24 h. After cultured islets were preincubated with 2·8 mM glucose for 30 min, they were incubated with 2·8 and 16·7 mM glucose for 90 min with or without 100 nM antimycin A. Values represent mean±S.E.M. of nine (glucose oxidation) and five (glucose utilization) determinations

	Control	100 nM antimycin A
Glucose oxidation		
2·8 mM glucose	9·8±0·5	9·8±0·7
16·7 mM glucose	42·1±1·8	32·8±1·8*
Glucose utilization		
2·8 mM glucose	32·9±3·3	31·1±2·4
16·7 mM glucose	97·9±5·6	76·7±6·5†

*$P<0·01$ versus control without antimycin A. †$P<0·05$ versus control without antimycin A.

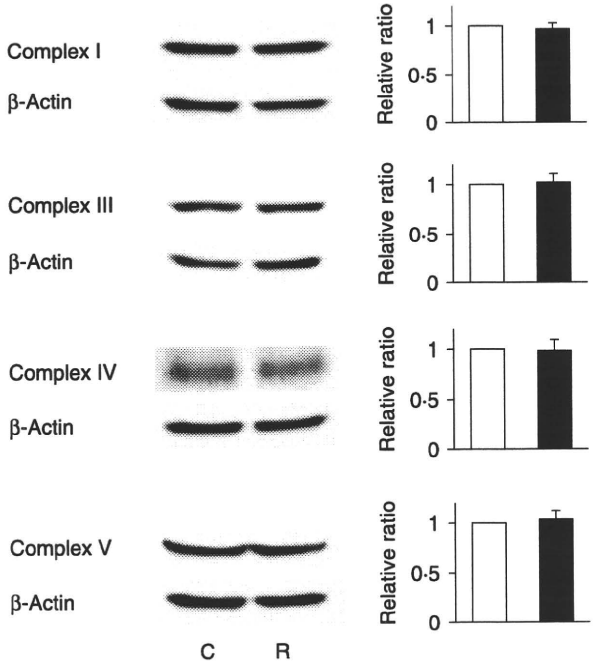

Figure 4 Immunoblots of complex I, III, VI, and V of mitochondrial respiratory chain proteins using lysates of whole-rat pancreatic islets. Islets were cultured with or without 30 nM rapamycin for 24 h. C, control; R, rapamycin. Quantification data from several independent experiments (I, $n=4$; III, $n=4$; VI, $n=3$; V, $n=4$) are also indicated. Open bar, control; closed bar, rapamycin. Data are expressed relative to control (without rapamycin) values corrected by β-actin level to eliminate influence of subtle difference in amount of loaded protein (means ± S.E.M).

succinate plus rotenone, TMPD plus ascorbate, and glycerol-3-phosphate. ATP production by mitochondria from rapamycin-cultured islets in the presence of pyruvate plus malate was decreased compared with that from control islets.

α-Keto-β-methyl-*n*-valeric acid (KMV), a specific competitive inhibitor of KGDH, dose dependently suppressed mitochondrial ATP production in the presence of malate and pyruvate (Fig. 5).

Effect of rapamycin on activities of mitochondrial enzymes

Enzyme activities in the Krebs cycle including PDH, NAD-ICDH, aconitase, and MDH were not affected, but KGDH activity was reduced by rapamycin treatment (Table 4).

Discussion

In the present study, we show that rapamycin suppresses high glucose-induced insulin secretion from pancreatic islets by reducing mitochondrial ATP production through suppression of carbohydrate metabolism in the Krebs cycle, together with reduced KGDH activity. Thus, dysfunction in mitochondrial ATP production may be derived not from alteration in protein expression and dysfunction of the respiratory chain but from decreased KGDH activity that limits the velocity of carbohydrate metabolism in the Krebs cycle.

Rapamycin significantly decreased glucose-induced insulin release after 1 to several days exposure, as found in previous studies using rat islets (Bell *et al.* 2003) and mice islets (Zhang *et al.* 2006). In the present study, exposure to 30 nM rapamycin for 24 h reduced glucose-induced insulin release without affecting insulin and DNA content, which indicates that reduced insulin release by rapamycin is not necessarily derived from reduced β-cell mass, while rapamycin above 10 nM was found to increase apoptosis in MIN-6 cells in a previous study (Bell *et al.* 2003). To investigate the mechanism of reduced insulin release by rapamycin independent of reduced insulin and DNA content, we used 30 nM rapamycin-treated islets. The recommended trough concentrations of rapamycin in blood are 5–15 ng/ml (or 5·5–15·9 nM) in islet transplantation (Shapiro *et al.* 2000) and renal transplantation (Teutonico *et al.* 2005). Accordingly, the concentration used in our experiments was two to six times clinically used trough concentrations.

In pancreatic β-cells, intracellular ATP originated mainly from mitochondria is one of the most important regulators of insulin secretion (Maechler & Wollheim 2001). Glucose entry into the β-cells accelerates glycolysis and mitochondrial carbohydrate metabolism that increases ATP content and ATP/ADP ratio, which closes the ATP-sensitive K^+ channels (K_{ATP} channel). The decrease in K^+ conductance depolarizes the membrane and opens the voltage-dependent Ca^{2+} channels (VDCCs). Increased Ca^{2+} influx through VDCCs increases the intracellular Ca^{2+} concentration to a level that triggers

Table 3 ATP production by mitochondria from control and rapamycin (Rp)-cultured islets. Islets were cultured with or without 30 nM Rp for 24 h. Mitochondrial suspension was obtained from control and Rp-cultured islets. Mitochondrial ATP production is indicated as the ratio to ATP production from adenylate kinase, which was determined from the same sample in parallel incubation. Values represent mean ± S.E.M. of five (A) and three (B) determinations

	Mitochondrial ATP production	
Experimental conditions	Control islets	Rp-cultured islets
A		
1 mM succinate+1 μM rotenone	6·40±0·32	6·47±0·44
1 mM pyruvate+1 mM malate	3·22±0·10	2·69±0·11*
0·5 mM TMPD+2 mM ascorbate	8·74±1·44	8·70±1·34
1 mM glycerol-3-phosphate	0·66±0·13	0·55±0·08
1 mM succinate+1 μM antimycin A	0·02±0·00	0·02±0·00
B		
1 mM succinate	7·13±0·12	ND
1 mM succinate+1 μM rotenone	6·39±0·06	ND
1 mM succinate+1 μM antimycin A	0·02±0·01	ND
1 mM succinate+1 μM rotenone+1 μM antimycin A	0·03±0·00	ND

*$P<0·05$ versus corresponding control cultured without Rp. TMPD, tetramethyl-*p*-phenyldiamine. ND, not determined.

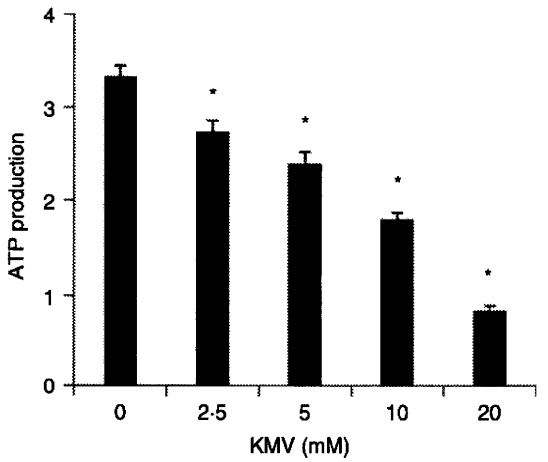

Figure 5 Effect of α-keto-β-methyl-*n*-valeric acid (KMV) on mitochondrial ATP production. Islets were cultured for 24 h. Mitochondrial suspension was obtained from cultured islets. Mitochondrial ATP production in the presence of 1 mM pyruvate and 1 mM malate with various concentrations of KMV is indicated as the ratio to ATP production from adenylate kinase, which was determined from the same sample in parallel incubation. Values represent mean±S.E.M. of six determinations. *$P<0·01$ versus control without KMV.

exocytosis of the insulin granules. Moreover, ATP directly affects the exocytotic system and enhances insulin release in experiments using single β-cells (Rorsman 1997, Takahashi *et al.* 1999) and permeabilized islets (Fujimoto *et al.* 2002). Thus, a lower ATP level in the presence of high glucose plays a major role in the attenuation of insulin secretion from rapamycin-treated islets in response to high glucose.

In pancreatic islets, KIC is oxidized, enhancing ATP production and triggering insulin release (Malaisse *et al.* 1981), and two distinct mechanisms of KIC-induced insulin release are proposed. In one, KIC, which is converted to acetyl CoA via a branched chain α-keto acid dehydrogenase (BCKDH) -dependent pathway, enters into the Krebs cycle and is oxidized (Lenzen *et al.* 1982, 1985). In the other, KIC together with endogenous glutamate is converted to α-ketoglutarate via glutamate-keto acid transaminase (GKAT), which enters into the Krebs cycle and is oxidized (Gao *et al.* 2003). Because both BCKDH and GKAT are mitochondrial enzymes, KIC might well be metabolized within mitochondria without affecting cytosolic glycolysis, which is compatible with the results showing that inhibition of glycolysis by glucokinase inhibitor and glyceraldehyde-3-phosphate dehydrogenase inhibitor decreased glucose-induced insulin release, but did not affect KIC-induced insulin release (Radu *et al.* 2005). Reduced KIC-induced insulin release by rapamycin suggests that the decreased glucose metabolism may be derived from reduced mitochondrial carbohydrate metabolism.

Table 4 Effect of rapamycin (Rp) on enzyme activities in the Krebs cycle. Islets were cultured with or without 30 nM Rp for 24 h. Enzyme activities were measured using homogenates of mitochondrial fraction obtained from control and Rp-cultured islets. Values represent mean±S.E.M. of five determinations

	Enzyme activities (nmol/mg mitochondrial protein per min)	
	Control islets	Rp-cultured islets
PDH	10·64±0·38	10·98±0·38
Aconitase	10·83±0·78	9·77±0·78
NAD-ICDH	11·50±0·28	10·99±0·30
KGDH	13·82±0·84	10·08±0·82*
MDH	1116±37	1127±37

*$P<0·05$ versus corresponding control cultured without Rp. PDH, pyruvate dehydrogenase; NAD-ICDH, NAD^+ linked-isocitrate dehydrogenase; KGDH, α-ketoglutarate dehydrogenase; MDH, malate dehydrogenase.

Because rapamycin reduced glucose utilization in the presence of high glucose, which reflects the velocity of glycolysis (Meglasson & Matschinsky 1986), the activity of glucokinase, a rate-limiting enzyme in glycolysis (Matschinsky 1996), was examined. Since rapamycin treatment did not affect glucokinase activity in islets, the primary cause of reduced glucose oxidation by the treatment is not likely to be reduced the velocity of glycolysis. Indeed, in islets, glucose utilization is also reduced when glucose oxidation is decreased by respiratory chain inhibitors including site III inhibitor in our results and site VI inhibitor (Sener *et al.* 2007), suggesting that reduced glucose oxidation may decrease glucose utilization. Since glucokinase is a unique hexokinase, which lacks product inhibition (Matschinsky 2002), accumulation of glucose-6-phosphate by mitochondrial metabolic inhibition may not participate in glycolysis inhibition. Moreover, since K_m of glucokinase for ATP is about 0·5 mM, which is less than the estimated cytosolic ATP concentration with a basal level of glucose in β-cells (about 3 mM; Meglasson & Matschinsky 1984), a decrease in the cytosolic ATP concentration by mitochondrial metabolic inhibition may have little effect on velocity of glycolysis.

Mitochondrial ATP production is driven by the H^+ gradient across the mitochondrial membrane generated by transport of high-energy electrons in the respiratory chain. These electrons are derived from NADH and $FADH_2$ derived from the Krebs cycle in the matrix and/or transferred from the cytosol by the shuttle system. To find the defective site in mitochondrial carbohydrate metabolism in rapamycin-cultured islets, mitochondrial ATP production was examined in the presence of various substrates and inhibitors. As ATP production in the presence of glycerol phosphate was not affected, reduced function of the glycerol phosphate shuttle, which is observed in diabetic islets (Östenson *et al.* 1993), may not participate in the reduction of ATP production by rapamycin treatment. In the presence of rotenone, a complex I inhibitor, and succinate, which renders electrons indirectly to complex I via the Krebs cycle and directly to complex II, electrons are rendered to the respiratory chain via $FADH_2$ at complex II and not at complex I via NADH, which is derived from metabolism in the Krebs cycle. TMPD is an artificial